Implementation of an end-to-end model of the Gulf of Lions ecosystem (NW Mediterranean Sea). I. Parameterization, calibration and evaluation

Daniela Bănaru, Frederic Diaz, Philippe Verley, Rose Campbell, Jonathan Navarro, Christophe Yohia, Ricardo Oliveros-Ramos, Capucine Mellon-Duval, Yunne-Jai Shin

Implementation of an end-to-end model of the Gulf of Lions ecosystem (NW Mediterranean Sea). I. Parameterization, calibration and evaluation

Bănaru Daniela*[1], Frédéric Diaz*[1], Philippe Verley[2], Rose Campbell[3], Jonathan Navarro[1], Christophe Yohia[1], Ricardo Oliveros-Ramos[4], Capucine Mellon-Duval[5], Yunne-Jai Shin[6]

[1]Aix Marseille Université, Université de Toulon, CNRS, IRD, MIO UM 110, Mediterranean Institute of Oceanography, Marseille, France.

[2]IRD, UMR 123 AMAP, TA40 PS2, Boulevard de la Lironde, 34398 Montpellier Cedex 5, France.

[3]Ecole d'Ingénieurs en Génie des Systèmes Industriels (EIGSI). 26, rue François de Vaux de Foletier, 17041 La Rochelle cedex 1.

[4]Instituto del Mar del Perú (IMARPE), Gamarra y General Valle s/n Chucuito, Callao, Peru.

[5]UMR MARBEC (IFREMER, IRD, UM, CNRS), 34203 Sète cedex, France.

[6]IRD, UMR 248 MARBEC, Université de Montpellier, Bat. 24 – CC 093 Place Eugène Bataillon 34095 Montpellier Cedex 5, France.

*Corresponding Authors: Tel: +33 (0)486 090 625 (D. Bănaru) : +33 (0)486 090 564 (F. Diaz)

Email addresses: daniela.Bănaru@univ-amu.fr (D. Bănaru), frederic.diaz@univ-amu.fr (F. Diaz),

--

Key words: ecosystem modelling, food web, fisheries, OSMOSE, Eco3M

*Note: This manuscript is linked to the manuscript: "***Implementation of an end-to-end model of the Gulf of Lions ecosystem (NW Mediterranean Sea). II. Investigating the effects of high trophic levels on nutrients and plankton dynamics and associated feedbacks through a two-ways coupling approach***" by Diaz et al. (2019). Ecological Modelling 405, 51-69, https://doi.org/10.1016/j.ecolmodel.2019.05.004*

ABSTRACT

An end-to-end model named OSMOSE-GoL has been built for the Gulf of Lions, the main French Mediterranean fishing area. This spatialized dynamic model links the coupled hydrodynamic and biogeochemical model Eco3M-S/SYMPHONIE (LTL - low trophic level model) to OSMOSE (HTL - high trophic level model). It includes 15 compartments of living organisms, five from the LTL model (*i.e*. nanophytoplankton, microphytoplankton, nanozooplankton, microzooplankton and mesozooplankton) and ten from the HTL model (northern krill, southern shortfin squid, European pilchard, European anchovy, European sprat, Atlantic horse mackerel, Atlantic mackerel, blue whiting, European hake and Atlantic bluefin tuna). With the exception of northern krill and European sprat, all HTL species are commercially exploited and undergo fisheries mortality pressure. The modeled species represent more than 70% of annual catches in this area. This paper presents the parameterization, calibration and evaluation of this model with satellite data for phytoplankton and with biomass, landings, diet and trophic level data for HTL groups. For most species, the diets in output of OSMOSE-GoL are similar to field and literature data in terms of dominant prey groups and species. However, some differences were observed. Various reasons may explain the mismatch between the modelled diet and field data. Benthic prey sometimes observed in the stomach content of the HTL predators were not modelled in OSMOSE-GoL. Field studies were carried out at specific periods and locations, while our data concern the period 2001-2004 and the entire modelled domain. Inter- and intra-annual variations in spatial distribution and density of prey may also explain these differences. The model estimates trophic level values similar to those cited in the literature for all the HTL compartments. These values are also close to the trophic levels estimated by a previous Ecopath model for the same area and period. Even though some improvements are still possible, this model may already be of use to explore fishery or Marine Protected Areas scenarios for socio-ecosystem management issues.

1. Introduction

End-to-end (E2E) models are particularly appropriate to disentangle the intricacy of interactions occurring between physical forcing and low and high trophic level communities in the context of a quantitative approach dedicated to Ecosystem-Based Management (EBM) (*e.g.* Travers et al., 2007; Rose, 2012). They use multiple field data sets and are able to assess and simulate the dynamics of the main descriptors of the ecosystem rather than evaluating single resources and single threats (Shin et al., 2010; Christensen and Walters, 2011; Collie et al., 2016). Similar approaches, driven by modeling and information are used not just in ecology, but in many other areas to improve, and in some cases save our lifes (Helbing et al., 2015).

However, the implementation of end-to-end modelling remains challenging, mainly due to the major differences between the sub-models of hydrodynamics and Low Trophic Level (LTL) organisms on the one hand, and that of High Trophic Level (HTL) organisms on the other hand (see review by Rose et al., 2010). The challenges are numerous and concern both concepts (*e.g.* representation of the zooplankton key level, differential scaling of processes, behavioral movement of HTL organisms, *etc.*) and technical issues (e.g. different programming languages and time-steps). One of the main challenges concerns the nature of link between sub-models. Travers et al. (2009) considered two possible types of links between LTL and HTL models. In the one-way forcing mode, LTL groups' biomasses serve as prey fields to HTL groups, without any feedback on the LTL compartments. In the two-ways coupling mode, the biomass of the LTL groups serve as prey field for HTL groups and an explicit rate of HTL-induced predation is specifically applied as feedback on each of the LTL groups.

Over the last decade, E2E modelling studies applied to regions or to the whole basin of the Mediterranean Sea have flourished in the context of EBM (Coll and Libralato, 2012). This research trend has been mainly driven by the more and more numerous observations of increasing threats and impacts on the Mediterranean marine ecosystems due to the exponential development of anthropogenic activities (*e.g.* Lötze et al., 2011; Coll et al., 2012). Most of these modelling studies

80 have been based on the Ecopath with Ecosim (EwE) model (see review of Coll and Libralato,
81 2012), and only a few have used alternative models, spatial and multispecies models such as the
82 OSMOSE size-based model (Halouani et al., 2016), or age-structured models applied to single
83 species (*e.g*. Santojanni et al., 2005).
84 Furthermore, while implementation of the EBM of the Gulf of Lions (GoL) is particularly crucial
85 owing to its major contribution to Mediterranean fisheries catches (S□cchi, 2008; Demaneche et al.,
86 2009), this shelf area has been poorly investigated to date (Coll and Libralato, 2012). Only the
87 recent study by Bănaru et al. (2013) dealt with the fishing impact on the trophic structure of the
88 marine ecosystem using an EwE approach. However, this study is not spatialized and is based on
89 some crude assumptions, concerning for example the plankton compartment (prey for the
90 planktivorous fish species), for which the biomass level is determined from the literature and
91 satellite imagery. A major bias of this type of modelling approach is that it does not account for the
92 close coupling between the physical and biological (*sensu largo*) processes. Yet these interactions
93 occur at multiple spatial and temporal scales in the NW Mediterranean Sea, and it has now been
94 well-demonstrated that they have a significant impact on the dynamics and the spatial distribution
95 of marine organisms from plankton to top predators (*e.g*. Fromentin et al., 2003; Niewiadomska et
96 □l., 2008; Cotté et □l., 2011; C□mpbell et □l., 2013). It is therefore necessary to represent the Gulf of
97 Lions ecosystem more realistically, in particular the environmental forcing, the spatial dynamics of
98 living organisms and their interactions, to enable a finer analysis of the functioning of the
99 ecosystems and *in fine* to plan its optimal management for the next decades.
100 The E2E approach developed in this study is based on a fully dynamic coupling (*i.e.* two-ways
101 coupling) of two pre-existing sub-models representing the dynamics of LTL organisms driven by
102 hydrodynamics and climate processes on the one hand, and the dynamics of HTL organisms
103 impacted by fishing activities on the other hand. The first model component is the Eco3M-
104 S/Symphonie model that has been successfully used in the North-Western Mediterranean Sea to
105 advance our understanding of the influence of hydrodynamics and atmospheric drivers on the

distribution of plankton at different spatial and temporal scales (*e.g.* Auger et al., 2011, 2014; Campbell et al., 2013; Carlotti et al., 2014). The second component model is the individual- and size-based model OSMOSE (Shin and Cury, 2004). This HTL model has been applied worldwide in order achieve better understanding of the functioning of diverse marine ecosystems (*e.g.* Travers et al., 2006; Marzloff et al., 2009; Fu et al., 2013; Grüss et al., 2015, 2016; Halouani et al., 2016). The aim of the present paper is to document an E2E model developed for the GoL (the OSMOSE-GoL model) and based on dynamic feedback (two-ways coupling) between two pre-existing LTL and HTL sub-models. Numerous data sets available in this marine region have been used to calibrate and quantitatively evaluate both the LTL and the HTL modules of the OSMOSE-GoL model. An application of this model that consists in an analysis of the impacts of the predation pressure exerted by HTL planktivorous species on the spatial distributions, the structure of the LTL community and food webs controls is presented in a companion paper (Diaz et al., 2019).

2. Methods

2.1. The E2E modelling approach

The approach developed in this study is based on the coupling of two existing sub-models. The first is the Eco3M-S/Symphonie model (Campbell et al., 2013) that represents the dynamics of Low Trophic Level (LTL) organisms driven by hydrodynamics and climate processes. The second is the individual-based model OSMOSE (Shin and Cury, 2004; Grüss et al., 2015), that simulates the dynamics of High Trophic Level (HTL) organisms. Both models have been fully described in previous works, therefore only the main characteristics are given hereafter. They are coupled in two distinct modes (Figure 1). In the one-way forcing mode, the biomass outputs of the LTL model are provided as inputs for the OSMOSE model without any feedback on the LTL biomass. In the two-ways coupling mode, there is a dynamic feedback between the two models through the predation process: the biomass outputs of the LTL model are provided as inputs for the OSMOSE model, which provides in return an additional rate of predation by the HTL planktivorous organisms.

132

133 2.1.1. Description of the LTL model

134 The LTL model is composed of two coupled models: the Symphonie hydrodynamic model
135 and the Eco3M-S biogeochemical model (Campbell et al., 2013). The meteorological and
136 hydrodynamic processes influencing the spatial and temporal distributions of nutrients and plankton
137 were simulated by the Symphonie model (Marsaleix et al., 2008), a 3-D primitive equation, free
138 surface model, based on hydrostatic and Boussinesq approximation. This model has already been
139 used to successfully represent certain physical processes in the Northwestern Mediterranean Sea
140 (*e.g*. Dufau-Julli nd et l., 2004; Ulses et l., 2008; Kersalé et al., 2013). The Symphonie version
141 used here has been developed by Hu et al. (2011a). The modeled zone (711 km by 303 km) extends
142 over the NW Mediterranean Sea, including the whole of the Gulf of Lions and parts of the Ligurian
143 and Catalan Seas (Fig. 2). The grid used a square horizontal mesh with a spatial resolution of 3 km
144 by 3 km. Sigma coordinates were used on the vertical dimension with a maximum of 40 levels. The
145 model was run from January 9, 2001 to December 24, 2004. All details on the initial and boundary
146 conditions are given in the studies of Hu et al. (2011a) and Campbell et al. (2013).
147 The biogeochemical model Eco3M-S is embedded in the Eco3M platform (Baklouti et al., 2006a,b),
148 and is a multi-nutrient and Plankton Functional Types (PFT) model that simulates the dynamics of
149 several biogeochemical decoupled cycles of biogenic elements (carbon, nitrogen, phosphorus and
150 silica) and non-redfieldian plankton groups. The Eco3M-S version has been recently used and
151 validated in the studies of Hu et al. (2011a,b) and Campbell et al. (2013) for the biogeochemical
152 components and the hydrodynamics features, respectively. The model structure encompasses seven
153 compartments of living organisms. Two of the three PFT of autotrophs of the model, from the
154 smallest to the largest, were accounted for: (1) nano-phytoplankton, NANOPHY (2–20 μm) that
155 dominate the biomass of phytoplankton assemblages for most of the year (Marty et al., 2002; Marty
156 and Chiavérini, 2010), with a heterogeneous taxonomic composition (*e.g.* autotrophic dinobionts);
157 and (2) the micro-phytoplankton community, MICROPHY (20-200 μm), largely dominated by

158 phytoplankton silicifiers (mainly diatoms) that can for certain periods contribute to a significant part
159 of primary production and biomass during spring bloom in the NW Mediterranean Sea (Marty et al.,
160 2002; Marty and Chiavérini, 2010). Three of the four PFTs of heterotrophs of the model, from the
161 smallest to the largest, were considered: (1) nano-zooplankton, NANOZOO (5-20 μm, mainly
162 bacterivorous dinobionts and small ciliates) that consume the smallest phytoplankton groups (<2
163 μm) and bacteria; (2) micro-zooplankton, MICROZOO (20-200 μm, mainly most of ciliates groups
164 and large dinobionts), having characteristics (growth, ingestion rates) close to NANOZOO but with
165 a wider prey spectrum, especially with potential consumption of micro-phytoplankton; and (3)
166 meso-zooplankton, MESOZOO (>200 μm, mainly copepod groups but also including amphipods)
167 grazing on the largest categories of plankton (>20 μm, micro-phytoplankton and micro-
168 zooplankton) and producing fast-sinking fecal pellets. All the formulations of the biogeochemical
169 processes, as well as the whole set of parameters, have been extensively described in Campbell et
170 al. (2013). Constant mortality rates were applied to some of phytoplankton and zooplankton groups
171 (Table 1), representing either senescence or viral attacks or predation.
172
173 2.1.2. Description of the HTL model
174 The OSMOSE (Object-oriented Simulator of Marine ecOSystEms, Shin and Cury, 2001;
175 Shin and Cury, 2004) model (version Osmose 3.2, www.osmose-model.org/downloads) is a two-
176 dimensional spatially explicit, individual-based model (IBM), written in Java (www.osmose-
177 model.org), and based on the main assumption of opportunistic and size-based predation. OSMOSE
178 is a multispecies model representing the whole life cycle of several interacting species, from eggs
179 and larvae to juveniles and adults. At the first time step following the production of eggs, the total
180 number of eggs of each population is split into super-individuals called “schools”, spatially
181 distributed according to the input distribution maps.
182 At each time step, OSMOSE simulates the biological and ecological processes at the super-
183 individual level: growth, predation and forage, reproduction, natural and starvation mortalities as

184 well as fishing mortality (Figure 1). The different sources of mortality of schools (fishing,
185 predation, starvation and diverse mortality) occur in a random order. Two types of movements are
186 considered in the OSMOSE-GoL model: (1) ontogenetic and seasonal migrations, taken into
187 account through the use of distribution maps; and (2) small-scale random diffusion, when the
188 distribution maps of schools (depending on fish age, stage, size, and season, year) does not change
189 from one time step to the next.
190
191 2.1.3. Technical details on the two-ways coupling mode
192 The two-ways coupling between the OSMOSE-GoL and Eco3M-S/Symphonie models was
193 performed through the predation process. Outputs of plankton groups provided by the LTL model
194 serve as prey fields for the HTL organisms, which return an additional predation mortality in the
195 plankton groups. To circumvent the different spatial dimensions (3D *vs*. 2D) and units (mmolN (or
196 C) m^{-3} *vs*. tons wet weight) of the two models, plankton concentrations were vertically integrated
197 and converted into biomass using conversion factors (Table 1). Only a small portion of plankton
198 biomass is available to fish and macroinvertebrates due to various processes affecting their vertical
199 distribution (turbulence, migrations, *etc*.). Availability of plankton to HTL species is not easy to
200 assess in the field, and literature on this point is non-existent. Therefore, the availability parameters
201 $\boldsymbol{a}_p$ (*p* for a given plankton group *p*) were estimated (Table 2) *via* the calibration of the model (see
202 hereafter).
203 The two-ways coupling mode meant that the HTL model returns a specific mortality rate for each
204 plankton group over space and time, and these rates were computed from the amount of prey
205 ingested, as described in Travers et al. (2009). In each cell (x,y) of OSMOSE-GoL and for each
206 plankton group (*p*), the HTL-induced mortality rate at time $t+\Delta t$ was computed as the total biomass
207 of plankton eaten ($\boldsymbol{BE}_{\Delta t}$) during the time step Δt (15 days) over the mean total plankton biomass
208 (*B*) at time *t* multiplied by Δt (Eq. (1)). As the maximum biomass of plankton *p* eaten by HTL
209 organisms at time $t+\Delta t$ is the available biomass $\boldsymbol{a}_p \cdot \boldsymbol{B}(\boldsymbol{x}, \boldsymbol{y}, \boldsymbol{t}, \boldsymbol{p})$ *at time t*, the HTL-induced

mortality rate can thus vary between 0 and $\frac{\alpha_p}{\Delta t}$. Because this variable mortality was added to the natural mortality (m_p) already considered in the Eco3M-S model (Table 1), the latter rate was reduced to ($\mu_p - \frac{\alpha_p}{2 \cdot \Delta t}$), with ($\frac{\alpha_p}{2 \cdot \Delta t}$) being the median of the variable mortality due to HTL species. It was not set to zero in order to account for other sources of mortality such as predation by non-modelled organisms, senescence and starvation mortality. Outside the common domain between the Eco3M-S/Symphonie and OSMOSE-GoL models (Figure 2), the plankton mortality rate was set to μ_p.

$$\mu(x, y, z, t + \Delta t, p) = \frac{BE_{\Delta t}(x, y, p)}{\Delta t \cdot B(x, y, t, p)} + \left(\mu_p - \frac{\alpha_p}{2 \cdot \Delta t} \right) \quad (1)$$

According to the equation (1), the plankton total mortality rate thus ranges between $\mu_p - \frac{\alpha_p}{2 \cdot \Delta t}$ and $\mu_p + \frac{\alpha_p}{2 \cdot \Delta t}$. This rate can be either lower or higher than the initial mortality rate μ_p depending on the predation pressure induced by HTL organisms.

2.1.4. Design of the numerical experiment

A first spin-up period of 35 years was launched in the one-way forcing mode to reach equilibrium of the HTL model outputs. This step was achieved using the numerical fields of plankton biomass in 2001. Following this period of spin-up, the model was then run in the one-way forcing mode (years 36 and 39) using the plankton biomass in 2001, and then in the two-ways coupling mode for four years (40 to 43). For the last four years (40 to 43), the HTL model received the numerical fields of LTL biomass for the years 2001 to 2004. These years was chosen because the LTL model has been previously validated over this period (Campbell et al., 2013). The coupling simulation started on January 10, 2001 (00h00) and it ended on December 20, 2004 (00h00). Years 36 to 39 (one-way forcing) as well as the period of two-ways coupling mode (years 40 to 43) were

232 considered for analysis hereafter. Furthermore, a set of 50 replicated simulations was run to account
233 for the stochasticity of the OSMOSE model.
234
235 2.2. Parameterization of the HTL model
236 2.2.1. Modelled domain and selected HTL groups
237 In this study, the OSMOSE-GoL model grid consists of 19 by 15 cells with a resolution of
238 12 km by 12 km covering the GoL area north of a line running from 42°04'-3°18' to 43°05'-5°37'
239 (Figure 2). A set of 25 schools released per time step per species (600 per year per species) was
240 chosen for this model as a compromise between the stochasticity of the model and numerical
241 limitations in memory and calculation speed.
242 As simulations with OSMOSE necessitate extensive information on entire life cycles, only 10 HTL
243 key species, being the most representative of the pelagic and demersal food web, were included in
244 the configuration of OSMOSE GoL: northern krill (*Meganyctiphanes norvegica*, (Sars 1857)),
245 southern shortfin squid (*Illex coindetii*, (Vérany 1837)), and eight fish species from small pelagic
246 fish to demersal fish: European pilchard (*Sardina pilchardus,* (Walbaum 1792)), European anchovy
247 (*Engraulis encrasicolus,* (Linnaeus 1758)), European sprat (*Sprattus sprattus,* (Linnaeus 1758)),
248 Atlantic horse mackerel (*Trachurus trachurus,* (*Linnaeus 1758*)), Atlantic mackerel (*Scomber*
249 *scombrus,* (Linnaeus 1758), blue whiting (*Micromesistius poutassou,* (Risso 1827)), European hake
250 (*Merluccius merluccius,* (Linnaeus 1758)), Atlantic bluefin tuna (*Thunnus thynnus,* (Linnaeus
251 1758)). These species represent more than 70% of annual catches (Demaneche *et al.*, 2009). Some
252 of them were selected because of their importance for fisheries (European pilchard, European
253 anchovy, Atlantic horse mackerel, Atlantic mackerel, European hake, Atlantic bluefin tuna) (SIH,
254 2017), others for their importance as forage species such as northern krill, European sprat and blue
255 whiting (Bănaru et al., 2013). All these species represent the most important ones in terms of
256 structure and functioning of the food web in this area (Bănaru et al., 2013).

To parameterize the model, various input information items were needed, including: (1) spatial distribution maps for different life stages and time steps (Appendix 1). These maps coded for presence *vs*. absence for each species. They have been obtained from geo-referenced data of the PELMED and MEDITS research surveys conducted since 1993 (IFREMER databases). Atlantic bluefin tuna is the sole highly migratory species with only a seasonal presence in the modelled area and not reproducing in the GoL (Imbert et al., 2007); (2) predation, growth and reproduction parameters (Table 4); (3) mortality parameters (Table 1); (4) fishing and reproduction seasonality (see sections 2.2.2 and 2.2.3).

2.2.2. Predation, growth and reproduction processes

In the OSMOSE model, predation is assumed to be an opportunistic process and occurs when there is both size adequacy and spatio-temporal co-occurrence between predator and prey. Within a cell of the grid, a predator can feed on a co-occurring prey if: (1) the prey is of a suitable size, that is, within a range determined by the minimum and maximum predator/prey size ratios; and (2) the vertical distribution of the prey makes it accessible to the predator, which is determined by the accessibility coefficients provided to OSMOSE-GoL. Therefore, the food web (or diet matrix) builds up as an emergent property of local trophic interactions (Travers et al., 2009). Minimum and maximum predator/prey size ratios (Table 3) were parameterized differently for different size classes for each taxon, in order to account for ontogenetic changes in feeding behavior. These size ratios were built from local data on diet, predators and prey size (Labat and Cuzin-Roudy, 1996; Båmstedt and K□rlson, 1998; Imbert et □l., 2007; Le Luherne, 2012; Bourgogne, 2013; Le Bourg et □l., 2015; Mellon-Duval et al., 2017).

The accessibility coefficients were set by default at 0.8 for HTL groups. For some species, these coefficients were reduced to 0.6 in relation to their exclusive benthic location during early life stages (northern krill <1 cm, southern shortfin squid <2 cm and European hake <6 cm), or to the very coastal area distribution patterns of individuals <5 cm and thus low accessibility to predation

283 (0.6 for European pilchard and anchovy and 0.4 for European sprat) (Labat and Cuzin-Roudy, 1996;
284 Mellon-Duval et al., 2017; Bănaru, pers. comm.; Bigot, pers. comm.).
285 During the predation process, if enough prey items are present in a spatial cell, a predator feeds
286 upon them uniformly until it reaches satiation. Predation efficiency is defined as the ingested prey
287 biomass over the maximum biomass a predator can feed upon. For each species, the maximum
288 ingestion rates (MIR, Table 3) have been assessed from local data (Palomares and Pauly, 1998;
289 Bănaru et al., 2013). However, some of the considered species consume a non-negligible part of
290 benthic prey that was not considered in the Osmose-GoL model. In order to avoid artificially
291 increasing predation on pelagic and demersal prey, their MIR were proportionally reduced by 35%
292 for southern shortfin squid, Atlantic horse mackerel, Atlantic mackerel and European hake (Kaci,
293 2012; Le Luherne, 2012; Mellon-Duval et al., 2017) and by 12.5% for blue whiting (Bourgogne,
294 2013). When the predator does not ingest enough food to fulfill its maintenance requirements
295 (corresponding to a predation efficiency threshold of 0.57; Shin and Cury 2004), fish starve at a rate
296 which decreases linearly with predation efficiency (Shin and Cury, 2004). The maximum mortality
297 rate by starvation was fixed at 1.0 $year^{-1}$, applied during a time step in the absence of food.
298 Predation efficiency also determines fish growth rate during a time step. When the biomass of prey
299 eaten is higher than maintenance requirements, the growth rate of fish is positive, varying as a
300 function of the von Bertalanffy growth rate and the predation efficiency (Shin and Cury, 2004).
301 The growth parameters (Table 4) were computed from local studies (Farrugio et al., 1991;
302 C□mpillo, 1992; SCRS, 1997; Mellon-Duval et al., 2009; GFCM-FAO, 2011a, b; PELMED and
303 MEDITS, IFREMER campaigns). Longevity was estimated from literature data (Campillo, 1992;
304 Labat and Cuzin-Roudy, 1996; Sánchez et al., 1998).
305 Predation success has also an indirect effect on the reproduction process through the biomass of
306 spawners which, combined with relative fecundity parameters, defines the number of eggs released
307 in the system. Any school of the key populations, whose size is greater than the sexual maturity size
308 (S_{mat}), reproduces according to the spawning seasonality and to the species relative annual fecundity

309 (φ, number of eggs spawned per gram of mature female per year) (Shin and Cury, 2004).
310 Data for size at maturity (S_{mat}) are indicated in Table 4 (Higginbottom and Hosie, 1989; F□rrugio et
311 al., 1991; C□mpillo, 1992; Labelle et al., 1997; Sánchez et □1., 1998; Lleonart, 2001; Sinovčić et al.,
312 2004; GFCM-FAO, 2011□, b; www.fishbase.org; PELMED and MEDITS, IFREMER campaigns).
313 Sex ratio was hypothetically fixed at 0.5.
314 The relative fecundity (Table 4) has been recomputed considering the number of eggs using data
315 from Ross and Quentin (1986), Campillo (1992), Laptikhovsky and Nigmatullin (1993), Qúero and
316 Vayne (1997), Sánchez et al. (1998), and the estimated weight of mature females based on the total
317 length for each species.
318 Seasonality of reproduction was estimated using data from Farrugio et al. (1991), Campillo (1992),
319 Labat and Cuzin-Roudy (1996), PELMED and MEDITS, IFREMER campaigns. Egg weight (0.54
320 mg) and size (S) (Table 4) were also indicated in the model (Qúero and Vayne, 1997; Le Bourg,
321 pers. comm.) as eggs represent potential prey for the rest of the food web.
322
323 2.2.3.Fishing and natural mortality processes
324 Fishing pressure is represented through a population-specific fishing mortality rate F (Table
325 2), affecting the number of fish per school when larger than the specified size of recruitment to
326 fisheries. Legal size of catch (S_{rec}, Table 4) has been used as recruitment size in the OSMOSE-GoL
327 model. Initial estimates of annual fishing mortality rates have been estimated for each target
328 species, using the landings to biomass ratio obtained from stock assessments (PELMED, MEDITS,
329 GCFM) and from the fisheries database (SIH, 2017). These mortality rates were subsequently
330 refined through the calibration of the model (see 2.3). Fishing mortalities are assumed to be
331 spatially homogeneous, but can vary seasonally as specified in input (Table 5). Fishing seasonality
332 was estimated using catch data by species (SIH, 2017).
333 In addition to explicit predation mortality modelled in Osmose, the mortality of the first life stages
334 (eggs and first feeding larvae, M_0, Table 2) is due to different natural causes (*e.g.* non-fertilisation of

335 eggs, starvation of first feeding larvae, advection, sinking) as well as predation by organisms not
336 considered in the OSMOSE-GoL model. Additional sources of natural mortality concerning other
337 life stages have also been accounted for (M_s, Table 2), including mortality due to disease,
338 senescence and predation by organisms not represented in the OSMOSE-GoL model (*e.g.* birds,
339 mammals, *etc.*). Since it is usually very hard to quantify these types of mortality, they have been
340 assessed through the calibration of the model for each of the ten HTL species.
341
342 2.3. Calibration for the HTL model
343 The OSMOSE-GoL model has been calibrated using an optimization technique based on an
344 evolutionary algorithm, and a maximum likelihood based objective function, so that the modeled
345 biomass and landings of the ten HTL species remained within realistic observed ranges. The data
346 sources used for the biomass are from the PELMED and MEDITS cruises performed every year in
347 June and July from 2000 to 2013 and GFCM-FAO stock assessments for the GoL (Jadaud, pers.
348 comm.; Bigot, pers. comm.; S□r□ux, pers. comm.), VPA models for hake and tuna (Jadaud, pers.
349 comm.; Fromentin, pers. comm.) and SIH (2017) for landings.
350 The calibration was performed with the calibraR package (Oliveros-R□mos et □l., 2015; Oliveros-
351 Ramos and Shin, 2016; https://CRAN.R-project.org/package=calibrar) that has been specifically
352 developed for calibrating complex ecological models, and osmose2R (http://www.osmose-
353 model.org, https://CRAN.R-project.org/package=osmose), which includes a set of R functions for
354 interfacing Osmose with calibraR.
355 The calibration step aimed at providing estimates of the following parameters of the model: (i)
356 availability coefficients of plankton groups to HTL species, (ii) larval mortality rate for each species
357 and (iii) fishing mortality rates for each species (Table 3). These parameters have been selected
358 because they are highly model-dependent, *i.e.* their meaning depends on the model structure and
359 assumptions, and there are no reasonable initial estimates for plankton accessibility and larval
360 mortality (Oliveros-Ramos et al., 2015). The objective function minimized by the algorithm is built

automatically by the R package by aggregating lognormal-likelihood functions that quantify the fit between model outputs and field observations. Biomass and landings from year 2001were given to the algorithm for every modeled species as the observed data, and the OSMOSE-GoL model was forced with the LTL biomass of the Eco3M-S/Symphonie model from the same year. In this way, a "steady-state" calibration of the OSMOSE-GoL model has been achieved for year 2001, that is the first year of the coupled simulation.

The calibration step enabled us to obtain a set of parameters so that biomass and landings of the considered HTL species best range between the minima and maxima of the observed biomass in the GoL. This parameter set was then used in the coupled model.

2.4. Datasets for the evaluation of the E2E model

2.4.1. Evaluating phytoplankton biomass of the LTL model using remote sensing satellite data

Ocean color data from the GlobColour project (www.glocolour.info/) were used in this study to evaluate the realism of the modelled surface chlorophyll *a* concentrations (considered as a proxy of phytoplankton biomass). The GlobColour product takes advantage of gathering data sets derived from several ocean color sensors (ENVISAT, MODIS, MERIS and SeaWiFs). Three sensors (SeaWiFS, MERIS and MODIS) showed a temporal overlap of functioning from April 2002 to December 2010, and it was possible to perform a quantitative comparison between satellite and modeled chlorophyll *a* values over most (990 days) of the modelled period (1440 days).

The GlobColour product provided a weighted mean ($\overline{Chl_w}$) and a weighted error ($\varepsilon\left(\overline{Chl_w}\right)$). The detailed computation of these parameters is given in the Product User Guide of GlobColour available on the aforementioned web site.

In order to accurately compare the concentrations of the satellite-derived chlorophyll *a* to those modeled, the numerical concentrations of total chlorophyll (sum of chlorophyll *a* concentrations of pico-, nano- and microphytoplankton) were averaged over the first optical layer (*sensu* Bricaud et al., 2010), $\overline{Chl_{opt1}}$. The details of the computation are given in the recent study of Campbell et al.

(2013). The model-derived chlorophyll *a* values were re-interpolated point by point at the size of each pixel (1.1 km) of the satellite image on the modeled domain. The period of assessment (990 days) was characterized by more than a third (~34%) of cloudy days without useable pixels on the modeled area, therefore the comparison was made on the remaining days, corresponding to a total of 236877 pixels.

A metric of model to data comparison (C parameter) was built and used hereafter. This metric assessed the size of the discrepancies between the predicted and satellite values as follows:

$$C=\begin{cases} 0, & if \quad \overline{Chl_{opt1}} \in \left[\overline{Chl_w} - \varepsilon\left(\overline{Chl_w}\right), \overline{Chl_w} + \varepsilon\left(\overline{Chl_w}\right)\right] \\ \min\left\{ \left| \overline{Chl_{opt1}} - \left(\overline{Chl_w} + \varepsilon\left(\overline{Chl_w}\right)\right) \right|, \left| \overline{Chl_{opt1}} - \left(\overline{Chl_w} - \varepsilon\left(\overline{Chl_w}\right)\right) \right| \right\}, & otherwise \end{cases}$$

2.4.2. Evaluating the HTL model using diet and trophic level data

Diet data for each of the modeled HTL species obtained as output of the OSMOSE-Gol model were compared with *in situ* field data obtained from stomach content analyses (Le Bourg et al., 2015; Bănaru, 2015; Bănaru, pers. comm.) or literature data (Båmstedt and Karlson, 1998; Sara and Sara, 2007; Mellon-Duval et al., 2017) for similar individual sizes.

Estimated trophic levels (TL) from the OSMOSE-Gol model were compared with TL values from the literature based on the stomach content (Båmstedt and Karlson, 1998; Stergiou and Karpouzi, 2002; Bănaru, 2015; Bănaru et Harmelin-Vivien, 2017) and compared with those of a local ECOPATH model (Bănaru et al., 2013).

The aim of these comparisons was to check whether the parameterization and the processes of the model were able to reproduce trophic interactions close to those observed in field data.

3. Results and discussion

3.1. Calibrated biomass and landings of the HTL model against data

The calibration of the model enabled us to estimate some parameters of the HTL model such

411 as the accessibility coefficients of the plankton and larval mortality of HTL species, and to refine the
412 fishing mortality estimates. The success of this calibration step lies in the ability of the model, once
413 run with this set of calibrated parameters, to provide results remaining within realistic ranges for the
414 biomass and landings of HTL species. The modeled median biomass (Figure 3) and landings (Figure
415 4) of the ten HTL species and their corresponding envelopes delimiting 0.25 and 0.75 percentiles are
416 presented for years 36 to 39 in the one-way forcing configuration. The modeled biomass and landings
417 for years 40 to 43, resulting from the two-ways coupling mode, are presented and discussed in the
418 companion paper (Diaz et al., 2019) for the detailed comparison with one-way forcing mode effects.
419 Most of the modeled biomass of HTL species showed seasonal patterns of change in median values
420 within the ranges of the field observations (Figure 3), except for that of European hake, which is
421 slightly overestimated. The biomass of certain species such as the European hake is known to be
422 underestimated, due mainly to the difficulty of catching large individuals during scientific surveys
423 (Bigot, pers. comm.). The median simulated biomass of northern krill (Figure 3A) showed a seasonal
424 dynamic with the highest values occurring in winter and the lowest at the end of the spring. The
425 seasonal patterns of change of southern shortfin squid (Figure 3B) showed median levels of biomass
426 around 2.5 x 10^4 tons, with maximum values at the end of summer and minimum values at the end of
427 winter. The stock of European pilchard (Figure 3C) showed cyclical variations around 2 x 10^5 tons,
428 with maxima reached in spring and minima at the beginning of the winter. The median biomass of
429 European anchovy (Figure 3D) showed cyclical seasonal variations centered on 10^6 tons, and
430 characterized by highest biomass from mid-winter to the end of spring, and the lowest during autumn.
431 The seasonal variation of the European sprat (Figure 3E) biomass was very low. The median levels
432 were around 1 x 10^4 tons, with a barely discernible peak at the end of summer. The seasonal dynamics
433 of Atlantic horse mackerel (Figure 3F) showed an increase in biomass at the end of autumn. A very
434 weak seasonal signal in the biomass of Atlantic mackerel was simulated (Figure 3G), with the highest
435 biomass extending from winter to mid–spring, and a minimum occurring from mid–summer to mid–
436 autumn. The biomass of blue whiting (Figure 3H) did not show any clear seasonal pattern and

437 oscillated around 4 x 10^4 tons. The temporal changes of European hake biomass (Figure 3I) also
438 showed a very weak seasonal signal, with values around 1.4 10^4 tons. By contrast, the biomass of
439 Atlantic bluefin tuna (Figure 3J) showed a marked seasonal cycle, with a minimum of biomass during
440 winter (~5 x 10^3 -5.5 x 10^3 tons), followed by a sharp increase to reach a first seasonal maximum at
441 the beginning of the spring (~5.6 x 10^3 - 6.2 x 10^3 tons). Another biomass minimum occurred at the
442 beginning of summer, and then the annual peak (around 7 x 10^3 tons) is observed in autumn. There
443 were no seasonal biomass field data to use for comparison with model output, as scientific surveys
444 were only organized during summer.
445 On the whole, for most of the HTL species, the whole or at least *pro parte* interannual dynamics of
446 modeled median landings (and the corresponding range of percentiles) were within the ranges of
447 observed data (Figure 4). However the median landings of southern shortfin squid (Figure 4B) and
448 of Atlantic mackerel (Figure 4F) were much higher than those observed, by a factor of 16 (~800 tons)
449 and 2.5 (~500 tons) with regard to observed landings, respectively, without any marked seasonal
450 pattern. A possible explanation for this discrepancy could be the underestimation of the landings of
451 southern shortfin squid and Atlantic mackerel in SIH (2017) landings databases, as for many other
452 demersal and benthic species, because fishermen often directly sell their fish at local markets
453 (CRPMEM PACA, 2016). Landings of northern krill and European sprat (Figures 4A and 4E) are not
454 computed by the model as they are not landed by fishermen. The simulated temporal dynamics of
455 planktivorous fish such as European pilchard and European anchovy showed marked and steady
456 seasonal cycles. The median landings for European pilchard (Figure 4C) were minimum (~180 tons)
457 at the beginning of winter. They rapidly increased during winter and reached a relative maximum
458 (~400 tons) at the beginning of spring. Then, they briefly fell below 400 tons and again increased up
459 to their absolute maximum (~750 tons) at the beginning of summer. They sharply decreased from the
460 middle of summer to the end of the autumn down the absolute minimum. Maximum simulated values
461 were higher than the maximum observed values during the first half of summer. The simulated
462 landings of European anchovy (Figure 4D) also showed a minimum (~100 tons) at the beginning of

463 winter, but the catch then increased very rapidly up to a first peak of ~180 tons, and an absolute
464 maximum (~250 tons) at the end of spring. The summer season is marked by a sharp decrease in
465 landings, and a third peak of landings (~200-220 tons) in autumn. The whole set of seasonal modeled
466 values remained within the range of observed landings. The seasonal changes in median landings for
467 Atlantic horse mackerel (Figure 4F) were characterized by two maxima in spring and autumn. The
468 spring maximum comprised between 20 and 28 tons was generally higher than the autumn maximum
469 (<20 tons). In parallel, minima (around 10 tons or lower) were simulated during winter and summer.
470 Only the maximum values of landings during spring and autumn fell within the range of observed
471 landings. The temporal patterns of change in simulated landings for blue whiting (Figure 4H) showed
472 a very marked seasonal trend. Median landings were close to zero from the beginning of summer to
473 the end of autumn, they sharply increased to reach ~40 tons at the beginning of spring, and then
474 drastically dropped during spring. The modeled landings were underestimated during the first half of
475 the year. The median landings of the European hake (Figure 4I) remained around 100 tons from mid-
476 winter to the end of summer within the range of observed landings during this period of year. They
477 fell sharply during autumn to well below the lower limit of observed data, with a minimum of ~10
478 tons, before increasing again at the beginning of winter. Modeled landings of Atlantic bluefin tuna
479 (Figure 4J) were close to zero only over a short period of the year, mainly from the end of autumn to
480 the beginning of winter. Catches sharply increased up to 250 tons during spring, before slightly
481 declining to just below 200 tons at the beginning of summer. Summer was marked by an abrupt
482 increase in the catches, reaching 500 tons at the end of summer. This seasonal cycle is characterized
483 by simulated landings that were close to field data.
484
485 3.2. Comparing phytoplankton surface biomass of the LTL model with ocean color data
486 The seasonal cycle of surface satellite-derived chlorophyll *a* content averaged over the
487 modeled area from April 2002 to December 2004 (Figure 5) is typical of those usually observed at
488 oceanic mid-latitudes (*e.g.* Siegel *et al.*, 2002), with average minima during summer months and

maxima from winter to late spring. The very low summer concentrations (~10^{-1} mg m^{-3} or lower) are considered as representative of the Mediterranean Sea (Bosc et al., 2004). As expected, the seasonal pattern found during the study period was close to the "bloom" trophic regime according to the classification of D'Ortenzio and Ribera d'Alcalà (2009) for the Mediterranean Sea.

An interannual variability of the seasonal cycle could be detected, with the year 2003 being characterized by a longer summer period of low chlorophyll *a* than 2002 and 2004. The year 2003 did not show any clear autumnal bloom, while it was particularly marked in mid-September 2002 and September and November 2004. The inter-annual variability in the phytoplankton surface content in this area of the Mediterranean Sea is a common feature that has been already observed in some other remote sensing time-series (Bosc et al., 2004; Auger et al., 2014) and in situ data (*e.g.* Marty and Chiavérini, 2010; Gernez et al., 2011).

Beyond the seasonal dynamics, the time-series highlights the variability of mean values at very high frequency (*i.e.* day-to-day), whatever the season considered. Most of the time, large error bars also suggest a strong spatial heterogeneity of phytoplankton content in the NW Mediterranean Sea. This variability at high frequency and the strong spatial heterogeneity are mainly due to the multiple physical forcing occurring in this marine area, such as changing wind gusts that drive intricate (sub)-mesoscale hydrodynamic processes (*e.g.* eddies, see Hu et al., 2011a,b) and upwellings (Millot, 1999), river inputs discharging large amounts of nutrients throughout the year (*e.g.* Minas and Minas, 1989) and the large-scale circulation of the Northern Current sometimes intruding on the shelf (Petrenko, 2003). All the aforementioned physical processes interact together at different spatial and temporal scales, and play a key role in setting ocean dynamics, heat transport and biogeochemical budgets through intense upwelling of nutrients, subduction of plankton and horizontal stirring (see review of Lévy, 2008).

The LTL model was able to reproduce the seasonal signal and the inter-annual variability of phytoplankton surface concentrations. The model also captured the daily variability. However, the modeled concentrations were, most of the time, underestimated compared to the satellite-derived

means concentrations, especially during late spring and summer. It is crucial to keep in mind that ocean color data in the Mediterranean Sea have to be considered with caution, because the algorithms used to derive the chlorophyll *a* concentrations perform poorly in this regional sea (Gregg and Casey, 2004; Volpe et al., 2007 and references therein). These low performances are generally attributed to the particular composition (*i.e.* inorganic and organic matter) of the water column causing an overestimation of chlorophyll *a* surface concentrations for low values especially of chlorophyll (i.e. during summer and in oligotrophic waters). This bias between *in situ* data and values derived from algorithms would be furthermore accentuated in the area of the Rhone freshwater influence according to the study of Ouillon and Petrenko, (2005). The C parameter, assessing error between model output and data (see section 2.4.2.), was null during *ca*. 23% of the comparison period. This result means that the modeled chlorophyll value remained within the range of the error bars given by the GlobColour algorithm during a quarter of the simulation period. Furthermore, figure 6 shows the temporal changes in the GlobColour errors on chlorophyll *a* concentrations and of the C parameter. The GlobColour errors and the C parameter were the lowest ($<1.25 \times 10^{-1}$ mg m^{-3}) during summer, especially in 2003 and 2004, when they were the most variable and highest from autumn to mid-spring. The C parameter was lower than the satellite sensor errors during *ca*. 71% of the comparison period, which is a rather satisfactory result.

3.3. Comparing modeled and observed diet of the HTL species

Figure 7 shows the modelled diet of every size class of the ten HTL species. In order to describe the diets emerging from the OSMOSE-GoL model, prey groups were classified into three categories according to their proportion (in biomass) in the predator's diet: main prey (>50%), secondary prey (from 10 to 50%), accessory prey (from 1 to 10%).

According to the model, the main prey of the Northern krill is microphytoplankton (~56%), while the secondary prey is microzooplankton (~35%). Mesozooplankton remains an accessory prey (~8%). This modelled diet, composed of phyto- and zooplankton in almost equal parts, is consistent

541 with the observations of Båmstedt and Karlson (1998) on krill of the Northeast Atlantic. According
542 to this field study, northern krill may not survive on a diet only based on phytoplankton and needs
543 to consume at least 40% of zooplankton.
544 The modelled southern shortfin squid mainly feeds on small teleosts (~77%) such as planktivorous
545 European pilchard (~36%) and European anchovy (~21%), but also on juveniles of Atlantic horse
546 mackerel (~9%) and blue whiting (~8%). Small squid (*i.e.* cannibalism) (~11%) are secondary prey,
547 while northern krill (~8%) and mesozooplankton (~4%) are accessory prey of southern shortfin
548 squid. This modelled diet is consistent with some *in situ* datasets (Bănaru, 2015) showing a diet
549 mainly composed by ~80% of teleosts. In the latter field study, southern shortfin squid prey on
550 certain other groups, such as benthic decapods, but these groups were not represented in the
551 OSMOSE-GoL model.
552 According to the model outputs, European pilchard larvae (<3 cm) mainly feed on
553 mesozooplankton (~81%). This trophic behaviour for larvae are close to the results of Borme et al.
554 (2009) in the Mediterranean Sea, showing a diet almost exclusively (~99%) composed of copepods
555 in the size range of mesozooplankton. Larger individuals significantly change their diet, feeding on
556 smaller prey, with microzooplankton (~51% of the diet of juveniles ranging between 3 and 12.5 cm,
557 and ~52% for adults >12.5 cm) as main prey, and microphytoplankton as secondary prey (~44% of
558 the diet of juveniles and ~43% for adults). The latter results are not in line with some recent dietary
559 field studies based on the analysis of stomach content in the Gulf of Lions. According to the study
560 of Le Bourg et al. (2015), juveniles of European pilchard as well as adults may prey quasi-
561 exhaustively on mesozooplankton (~98% and 100%, respectively). However this mismatch between
562 model outputs and observations has to be moderated, because the study of Bode et al. (2004)
563 showed that the size of the prey generally decreases with increasing body length of European
564 pilchard. Hence, adults may consume a larger part of phytoplankton according to the latter study. As
565 phytoplankton prey are actually more easily digested, they are therefore more difficult to identify in
566 stomach contents, which may explain the differences between the model and observations for this

fish species. Moreover, the study of Pethybridge et al. (2014) using analysis of fatty acids in adults of European pilchard confirms the assumption that its diet is mainly based on microplankton.

The modelled European anchovy, including its larvae stage, has a diet similar to those of the juveniles and adults of European pilchard. All stages mainly feed on microzooplankton (~55% of the diet for larvae <3 cm, ~49% for juveniles ranging between 3 and 12.5 cm and ~44% for adults >12.5 cm). Their secondary prey is the microphytoplankton group (~39% for larvae, ~40% for juveniles and ~36% for adults). Mesozooplankton is only an accessory prey, representing about 5% of the diet for larvae and juveniles, and around 7% for adults. The simulated diet of the larvae is close to observed data. Analyzing fatty acids content, Rossi et al. (2006) showed that microzooplankton and microphytoplankton are the prey most consumed by anchovy larvae. However, the modelled diet for adult anchovy is rather different from those resulting from the analysis of stomach content (Borme et al., 2009; Le Bourg et al., 2015). In the observations, as for the European pilchard, the proportions of microzooplankton and microphytoplankton may be underestimated due to a rapid digestion of these types of prey.

The modelled diet of European sprat juveniles is similar to those of juveniles and adults of the European pilchard and of all size classes of the European anchovy. The diet of the juveniles is composed of microzooplankton (~48% of the diet) and microphytoplankton (~34%). The proportion of consumed mesoozooplankton (~14%) is higher than in the diet of the juveniles of the European sardine and anchovy, but is much lower than that observed in their stomach content (~100%), according to the study of Le Bourg et al. (2015). The modelled diet of European sprat larvae (<3 cm) is mainly composed of mesozooplankton (~81%), which is consistent with previous observations (Dickmann, 2005). Mesozooplankton is furthermore the main prey for adults but in much higher proportions (~68%) than for the adults of European pilchard and anchovy (~4.5% and ~7%, respectively). Adults also consume, as secondary prey, some European pilchard larvae (~16%). In the model, the European sprat (including larvae and adults) thus appears to be more carnivorous than the European sardine and anchovy. This modelled output is in line with the dataset

of Pethybridge et al. (2014) based on the comparative analysis of the fatty acids content of these three pelagic species. In the model, pilchard eggs and larvae are another significant prey (~16%) for the adults of European sprat, as also observed in their stomach content (Le Bourg et al., 2015). The diet of the juveniles of Atlantic horse mackerel predicted by the model is composed of a dominant proportion of mesozooplankton (~62%) and a lesser proportion of fish larvae (~25%), while the study of Le Luherne (2012) based on the analysis of stomach content showed a dominant consumption of northern krill (~71% in proportion) and a lesser proportion (~21%) of benthic decapods (not modelled). These differences may result from opportunistic predation behaviour (making the diets highly variable between the sampling stations inside the GoL domain), as well as from some differences between the spatial domain of the model (entire GoL) and the specific locations of the sampling stations used in the study of Le Luherne (2012). Adults of Atlantic horse mackerel (>16 cm) have a modelled diet which is quite different from that of juveniles. They mainly feed on southern shortfin squid (~37%) and northern krill (~28%). Some other prey such as juveniles of European sprat and hake and Atlantic mackerel supplement their diet (~17%). The cumulated percentage of consumed fish is rather high (34%). The modelled proportion of northern krill consumed is close to that resulting from the analysis of *in situ* stomach content (~21%; Le Luherne, 2012). By contrast, the latter empirical study did not show the presence of southern shortfin squid in the stomach of analysed individuals. Differences between model outputs and observations may again result from differences in diet when estimated from the entire modelled domain rather than from some particular locations as in the study of Le Luherne (2012). Differences in the diet of predators may also result from inter- annual variations in the spatial distribution and density of prey. Furthermore, a major bias in the modelling of the diet of Atlantic horse mackerel adults is that a dominant proportion of consumed prey (~54% of macrozooplankton in the form of pteropods and ~21% of decapods, Le Luherne, 2012) is not represented as potential prey in the model.

In the model, the juveniles of Atlantic mackerel (<20 cm) mainly consume certain planktivorous

fish, a result which is consistent with observations (Le Luherne, 2012). However, the modelled diet appears to be dominated by European pilchard (~38%) and European anchovy (~22%), while the analysis of stomach content data rather shows a high consumption of sprats (~37%) and to a lesser extent, anchovies (~16%). Accessory prey are diverse (*i.e.* mesozooplankton, northern krill, southern shortfin squid, Atlantic horse mackerel, blue whiting, other prey), each of them accounting for 6 to 7% of the modelled diet. The differences in the consumed fish species between the model and observations may be attributable to differences in species composition between the modelled period (2001-2004) and the field studies that were carried out in 2011-2012 (Le Luherne, 2012). Since 2008, the biomass of European pilchard has strongly declined in the Gulf of Lions, while that of sprat has increased (Van Beveren et al., 2014). Macrozooplankton and groups of benthic species that are not represented in the model account for significant proportions of the stomach content (~27%, ~19% respectively, Le Luherne, 2012). The model succeeded in predicting the functional group consumed (*i.e.* planktivorous fish) for the juveniles of Atlantic mackerel. Adults of Atlantic mackerel (>20 cm) are even more piscivorous than juveniles, since their modelled diet is almost 90% composed of fish. The most consumed fish are firstly European pilchard (~46%) and secondarily, European anchovy (~26%), in the model. Comparatively, the proportion of consumed teleosts observed in stomach content amounts to almost 90% in the study of Le Luherne (2012), but the teleost species could not be identified due to too advanced digestion of prey.

Juveniles of blue whiting (<15 cm) have a rather diversified diet in the model. They feed on certain plankton groups (mesozooplankton at ~19%, and northern krill at ~25%), on southern shortfin squid (~10%) and on different species of fish (~46%). The most consumed fish species are European pilchard (~27%), Atlantic horse mackerel (~10%) and blue whiting (~6%). This result is different from those obtained in the study of Bourgogne (2013) who observed only decapods (not represented in the model) in the stomach content of analysed juveniles. In the model, adults of blue whiting (>15 cm) mainly feed on fish (~65%) secondarily on northern krill (~26%) and southern shortfin squid (~10%). The most preyed species of fish are European pilchard (~32%), Atlantic horse

mackerel (~11%), blue whiting (~12%) and European anchovy (~8%). The study of Bourgogne (2013) showed a proportion of northern krill (~33%) close to that provided by the model. The main difference between model and observations is in the dominant prey. The proportion of teleosts consumed amounts to ~65% in the model, while stomach content data show a lower proportion (~35%, Bourgogne, 2013). In parallel, benthic decapods (not modelled) have been found in a significant proportion (~32%) in the stomach content of analysed adults, which may explain the mismatch between the modelled diet of adults and field data.

In the model, the main prey of the European hake juveniles are teleosts (~90%). Among these teleosts, the most consumed species are firstly the European pilchard (~42%), secondly the European anchovy (~24%) and thirdly, the blue whiting (~13%). In parallel, a recent study of stomach content from the same area (Mellon-Duval et al., 2017) revealed *in situ* diet mainly composed of teleosts (>80% and to 100%). In more detail, the European pilchard was observed in the highest proportion (22 to 74%), but the European anchovy and the blue whiting were also detected in lesser proportions (6 to 30% and 1 to 3%, respectively). The model results also match the observations of two other recent studies, estimating at ~92% the proportion of teleosts in the diet of juveniles (Merquiol, 2016; Bănaru and Harmelin-Vivien, 2017). In the model, adults, as juveniles, feed mostly on teleosts (~93%). The teleost prey are firstly European pilchard in a proportion of ~43%, and secondly, blue whiting at ~13%. Other fish species such as European sprat, Atlantic mackerel and European hake supplement their diet up to 16%. Mellon-Duval et al. (2017) found from the analysis of stomach content a roughly similar proportion of European pilchard (~38%) and slightly higher proportion of blue whiting (~26 to ~30%).

The modelled diet of Atlantic Bluefin tuna is almost exclusively piscivorous (~93%) and composed of small teleosts. European pilchard is the main prey (~51%), while European anchovy (~23%) and blue whiting (~10%) are the secondary prey. Southern shortfin squid is only an accessory prey (~7%). This preference for planktivorous teleosts, mainly European anchovy, has already been shown from the analysis of the stomach content of individuals caught in the Gulf of Lions (Imbert

et al., 2007). Once again, the minor mismatches observed between the modelled diet and that from the field data may result from a dataset based on sampling carried out outside the temporal window of the simulation period. This fast-swimming pelagic tuna species has been shown to have a high variability in its distribution at different spatial and temporal scales in the GoL (Royer et al., 2004).

3.4. Comparing TL in the E2E modelled food web with literature data

The E2E modelled food web (Figure 8) is composed of 15 compartments organised into four trophic levels (TL). This food web length is rather common in natural ecosystems (Hastings and Conrad, 1979). Five plankton groups represent the lowest TL ([1-2]), while ten invertebrates and teleost groups represent the highest TL (>3). The highest flows of predation occur between the phyto- and zooplankton groups (>10^6 tons y^{-1}), and sharply decrease with increasing TL, which is a common feature observed in trophic pyramids (Odum, 1959). Primary producers such as nano- and microphytoplankton representing the first TL are mainly consumed by nano- (TL=2.0), micro- (TL=2.0) and mesozooplankton (TL=2.2). Among these groups, mesozooplankton has the highest TL, as it consumes both phyto- and zooplankton. Planktivorous species such as northern krill (TL=2.5), European pilchard (TL=2.7), European anchovy (TL=2.8) and European sprat (TL=2.9) mainly feed on micro- and mesozooplankton. The European pilchard has a more omnivorous diet, with a consumption of microphytoplankton of the same order of magnitude as that of microzooplankton, or even higher than that of mesozooplankton. For these planktivorous species, TL increases from the northern krill to the European sprat, in agreement with literature data (Båmstedt and Karlson, 1998; Stergiou and Karpouzi, 2002; Le Bourg et al., 2015).
Among the meso-predators, the Atlantic horse mackerel has the lowest TL (TL=3.5), followed by those of Atlantic mackerel (TL=3.9), southern shortfin squid (TL=4.0), blue whiting (TL=4.0), Atlantic bluefin tuna (TL=4.0) and European hake (TL=4.1). These TLs are close to field data (Stergiou and Karpouzi, 2002; Sara and Sara, 2007; Bănaru, 2015; Bănaru and Harmelin-Vivien, 2017; Mellon-Duval et al., 2017). Some larvae of these teleosts are consumed by cannibalism and

697 also by other species of similar, lower and higher TL.

698 On the whole, the modelled TLs are in agreement with literature data and ECOPATH-GoL outputs
699 for most of the 10 HTL species (Figure 9). Some interesting points can however be highlighted. The
700 modelled TLs of southern shortfin squid are slightly higher than those in the literature (Bănaru et
701 Harmelin-Vivien, 2017) and from ECOPATH outputs (Bănaru et al., 2013). The predator-prey size
702 ratios of the present model may be better adjusted in order to obtain a modelled TL for southern
703 shortfin squid closer to field and literature data.

704 The modelled TLs of juveniles and adults of European pilchard are close to the minimum values
705 estimated from the analysis of the stomach content (Stergiou and Karpouzi, 2002) or using $\delta^{15}N$
706 stable isotope ratios (Bănaru, 2015), while the corresponding larvae show their numerical TLs close
707 to the observed highest values. In this case too, the predator-prey size ratios of the model may be
708 better adjusted.

709 The TLs of all species (except pilchard, and to a lesser extent blue whiting) increase with increasing
710 size of individuals. In order to better account for ontogenetic changes in TL (Chassot et al. 2008;
711 Reed et al. 2017), it would be useful in the future to better refine field estimation of trophic levels
712 by size.

713 It is interesting and encouraging to note that the TLs computed from two very different approaches
714 of E2E modelling (*i.e.* OSMOSE *vs.* ECOPATH) are very close for most of HTL species, except for
715 European pilchard and blue whiting. Even if the represented periods in these models partly overlap
716 (2001-2004 for OSMOSE and 2000-2009 for ECOPATH) and the modelled area is the same, major
717 differences in conception between these two models (opportunistic, size-based diet in OSMOSE
718 and fixed diet in ECOPATH) may explain these small differences in trophic level results. OSMOSE
719 is an individual size-based, spatial and dynamic model, while ECOPATH is a mass-balanced model,
720 with no size groups, non-spatialized and offering a static snapshot of the system. Moreover,
721 ECOPATH includes more groups and species (benthic groups, marine mammals, birds and others),
722 which are not represented in OSMOSE. Data gaps concerning the diet of some species were

723 highlighted by Bănaru et al. (2013), and new recent diet data were included in the OSMOSE model
724 parametrization.
725
726 **4. Conclusion**
727 The GoL is a highly exploited area for fisheries (Demaneche et al., 2009; Bănaru et al., 2013). Here,
728 as in other parts of the world, fishing has reduced the biomass of top predators (Aldebert, 1997;
729 Piroddi et al., 2017), with potential cascading effects on the flows and biomass in the food web
730 (Pauly et al., 1998; Cury et al., 2003; Bănaru et al., 2010; Ferretti et al., 2010). Climate variations
731 impact the GoL ecosystems through river inputs (Ludwig et al., 2009) or hydrological processes
732 (Hermann et al., 2008). As shown in other areas, the impact of fishing combined with climate
733 changes induces sometimes unexpected effects in the ecosystems (Travers-Trolet et al., 2014; Auber
734 et al., 2015). The end-to-end modelling approach aims at understanding and anticipating some of
735 these processes.
736 This paper presents the first spatialized dynamic coupled end-to-end ecosystem model for the GoL.
737 The modeled groups and species represent more than 70% of annual catches in this area, and they
738 encompass the pelagic and demersal ecosystem trophic structure organised into four trophic levels.
739 The assessment of both LTL and HTL groups and species of the E2E OSMOSE-GoL model showed
740 a satisfactory agreement with literature, satellite and field local data in terms of biomass, landings
741 and diet. The model has been parametrized with the best available local data. Following the
742 calibration stage, realistic ranges for the biomass and landings have been obtained for most species
743 and groups. Biomass for the European hake and landings for the Atlantic mackerel are however
744 slightly overestimated. At first sight, it might be considered that these differences are acceptable
745 owing to uncertainties existing in biomass estimations and landings data. However, some
746 improvements of the model are obviously still possible. Predator-prey size ratios may be refined to
747 produce a better correspondence between model and field data. Sex-ratio established by default at
748 0.5 may be refined with field data when available. The distribution maps currently based on

749 presence-absence may be replaced with density-based maps. Fishing mortality considered uniform
750 for the entire domain may be also spatialized.
751 Previous versions of the OSMOSE model have already been applied in different ecosystems to
752 address various questions regarding: i/ the assessment of the ecosystem trophic structure (Marzloff
753 et □l., 2009; Grüss et □l., 2015; H□lou□ni et □l., 2016, Fu et □l., 2017), ii/ the effect of Marine
754 Protected Areas (Yemane et al., 2009), iii/ the combined effects of fishing and climate change
755 (Tr□vers et □l., 2009; Fu et □l., 2013; Tr□vers-Trolet et □l., 2014; Fu et al., 2018) iv/ the simulation
756 of fishing scenarios (Shin et □l., 2004; Tr□vers et □l., 2010; Smith et □l., 2011; Grüss et □l., 2016),
757 and v/ the testing of indicator performance (Travers et al., 2006; Shin et □l., 2018). However, the
758 present version of E2E OSMOSE for the GoL may go further, in the analysis of the fine impact of
759 the predation pressure exerted by HTL planktivorous species on the spatial distributions and the
760 structure (size, trophic shortcut, *etc*.) of the plankton community. It may also contribute to the
761 understanding of complex processes of simultaneous bottom-up and top-down controls in this
762 exploited ecosystem (Diaz et al., 2019). Moreover, this type of E2E model may allow for the
763 quantitative assessment of the combined effects of fishing and climate change scenarios on the
764 ecosystem dynamics and for the computation of model-based indicators used to assess whether an
765 ecosystem and its services are used sustainably, and then maintained (Coll *et al.*, 2015). The impact
766 of existing or future Marine Protected Areas (Gulf of Lions, Fisheries Restricted Area, *etc.*) and
767 spatio-temporal management measures on the structure and the functioning of the ecosystem may
768 also be tested in future.
769 This coupled E2E model may be extended to the entire Mediterranean Sea and compared with
770 existing Ecopath with Ecosim ecosystem model configurations (Coll □nd Libr□□to, 2012; Piroddi et
771 al., 2017).
772
773 **Acknowledgements**

774 This study was funded by the project EMIBIOS (End-to-end Modelling and Indicators for.
775 BIOdiversity Scenarios, FRB contract no. APP-SCEN-2010-II) and by the EU FP7 project
776 PERSEUS (Policy-oriented marine Environmental Research for the Southern European Seas,
777 Theme “Oceans of Tomorrow” OCEAN.2011-3 Grant Agreement No. 287600). It benefited from
778 and contributed to MERMEX WP2 collaborative work and to the MERMEX IPP “Interactions
779 plancton-planctonophages” project. We wish to thank J.M. Fromentin, J.L. Bigot, C. Saraux, A.
780 Jadaud for providing some data and expertise. The authors acknowledge T. Ballerini for her
781 contribution to the coupling code and suggestions that improved the parametrization of the
782 OSMOSE-GoL model, the assistance of staff maintaining the clusters DATARMOR of the
783 IFREMER and HPC Platform of the OSU Institut PYTHEAS (Aix-Marseille University, INSU-
784 CNRS) for providing the computing facilities, as well as for technical assistance. Thanks are also
785 addressed to Michael Paul for English corrections.
786

787 **References**
788
789 Aldebert, Y., 1997. Demersal resources of the Gulf of Lions (NW Mediterranean). Impact of
790 exploitation on fish diversity. Vie et Milieu 47, 275–285.
791 Auber, A., Travers-Trolet, M., Villanueva, M.C., Ernande, B., 2015. Regime Shift in an Exploited
792 Fish Community Related to Natural Climate Oscillations. PLoS ONE 10(7), e0129883.
793 https://doi.org/10.1371/journal.pone.0129883.
794 Auger, P., Diaz, F., Ulses, C., Estournel, C., Neveux, J., Joux, F., Pujo-Pay, M., Naudin J.-J., 2011.
795 Functioning of the planktonic ecosystem on the Gulf of Lions shelf (NW Mediterranean)
796 during spring and its impact on the carbon deposition: A field data and 3-D modelling
797 combined approach. Biogeosciences 8(11), 3231–3261. doi:10.5194/bg-8-3231-2011.
798 Auger, P-A., Ulses, C., Estournel, C., Stemmann, L., Somot, S., Diaz, F., 2014. Interannual control
799 of plankton ecosystem in a deep convection area as inferred from a 30-year 3D modelling

study: winter mixing and prey/predator interactions in the NW Mediterranean. Prog. Oceanogr. 124, 12-27. doi.org/10.1016/j.pocean.2014.04.004.

Baklouti, M., Diaz, F., Pinazo, C., Faure, V., Quéguiner, B., 2006a. Investigation of mechanistic formulations depicting phytoplankton dynamics for models of marine pelagic ecosystems and description of a new model. Progr. Oceanogr. 71, 1–33. doi:10.1016/j.pocean.2006.05.002.

Baklouti, M., Faure, V., Pawlowski, L., Sciandra, A., 2006b. Investigation and sensitivity analysis of a mechanistic phytoplankton model implemented in a new modular numerical tool (Eco3M) dedicated to biogeochemical modelling. Progr. Oceanogr. 71, 34–58. doi:10.1016/j.pocean.2006.05.003.

Båmstedt, U., Karlson, K., 1998. Euphausiid predation on copepods in coastal waters of the Northeast Atlantic. Mar. Ecol. Progr. Ser. 172, 149-168. doi: 10.3354/meps172149.

Bănaru, D., 2015. Pelagic and demersal foodweb of the Gulf of Lions elucidated by stable isotope analysis. MERMEX WP2, MISTRALS Workshop, Marseille, 20-22 octobre 2015.

Bănaru, D., Harmelin-Vivien, M., 2017. Résultats DCSMM obtenus lors des campagnes MEDITS et PELMED 2015 sur la façade Méditerranéenne ». Dans Mialet et al., 2017. Bilan des essais et optimisation du suivi mutualisé « réseaux trophiques et contaminants » sur les campagnes halieutiques DCF 2014-2015. Programmes de surveillance DCSMM « Poissons et Céphalopodes, contaminants, questions sanitaires » sur les plateaux continentaux, 112 pp (In French).

Bănaru, D., Harmelin-Vivien, M., Boudouresque, C.-F., 2010. Man-induced change in community control in the north-western Black Sea: the top-down bottom-up balance. Mar. Environ. Res. 69(4), 262-275. doi: 10.1016/j.marenvres.2009.11.009.

Bănaru, D., Mellon-Duval, C., Roos, D., Bigot, J.-L., Souplet, A., Jadaud, A., Beaubrun, P., Fromentin, J.-M., 2013. Trophic structure in the Gulf of Lions marine ecosystem (North-Western Mediterranean Sea) and fishing impacts. J. Mar. Syst. 111-112, 45-68. doi : 10.1016/j.jmarsys.2012.09.010.

826 Bode, A., Álvarez-Ossorio, M.T., Carrera, P., Lorenzo, J., 2004. Reconstruction of trophic pathways
827 between plankton and the North Iberian sardine (*Sardina pilchardus*) using stable isotopes.
828 Sci. Mar. 68, 165-178. doi.org/10.3989/scimar.2004.68n1165.
829 Borme, D., Tirelli, V., Brandt, S.B., Fonda Umani, S., Arneri, E., 2009. Diet of *Engraulis*
830 *encrasicolus* in the northern Adriatic Sea (Mediterranean): ontogenetic changes and feeding
831 selectivity. Mar. Ecol. Prog. Ser. 392, 193-209. doi: 10.3354/meps08214.
832 Bosc, E., Bricaud, A., Antoine, D., 2004. Seasonal and interannual variability in algal biomass and
833 primary production in the Mediterranean Sea, as derived from 4 years of SeaWiFS
834 observations. Global Biogeochemical Cycles 18(1), 1-17. doi:10.1029/2003GB002034.
835 Bourgogne, H., 2013 Etude de la stratégie alimentaire du *Micromesistius poutassou* (Risso, 1827)
836 dans le golfe du Lion (France). Rapport de stage Master 1 Océanographie, Aix-Marseille
837 Université, 8 pp.
838 Bricaud, A., Babin, M., Claustre, H., Ras, J., Tièche, F., 2010. Light absorption properties and
839 absorption budget of southeast pacific waters. J. Geophys. Res. 115, C08009.
840 doi.org/10.1029/2009JC005517.
841 Bundy, A., 2004. Mass balance models of the eastern Scotian Shelf before and after the cod collapse
842 and other ecosystem changes. Can. Tech. Rep. Fish. Aquat. Sci. 2520, 1488-5379.
843 Campbell, R., Diaz, F., Hu, Z., Doglioli, A., Petrenko, A., Dekeyser, I., 2013. Nutrients and
844 plankton spatial distributions induced by a coastal eddy in the Gulf of Lion. Insights from a
845 numerical model. Progr. Oceanogr. 109, 47-69. doi.org/10.1016/j.pocean.2012.09.005.
846 Campillo, A., 1992. Les pêcheries françaises de Méditerranée: synthèse des connaissances.
847 IFREMER RI DRV 92–019 RH/Sete. (http://archimer.ifremer.fr/doc/00000/1125/.) 206 pp.
848 Carlotti, F., Eisenhauer, L., Campbell, R., Diaz, F., 2014. Modelling spatial and temporal population
849 dynamics of the Copepod *Centropages typicus* in the North western Mediterranean Sea during
850 the year 2001 using a 3D ecosystem model. J. Mar. Syst. 135, 97-116. doi:
851 10.1016/j.jmarsys.2013.11.007.

852 Chassot, E., Rouyer, T., Trenkel, V.M., Gascuel D., 2008. Investigating trophic-level variability in
853 Celtic Sea fish predators. J.Fish Biol. 73, 763-781. Doi: 10.1111/j.1095-8649.2008.01938.x.
854 Christensen, V., Walters, C.J., 2011. Progress in the use of modeling for fisheries management. In
855 Ecosystem Approaches to Fisheries: A Global Perspective, Eds. Christensen, V., Maclean, J.
856 L., Cambridge University Press. 189-205.
857 Coll, M., Libralato, S., 2012. Contributions of food web modelling to the ecosystem approach to
858 marine resource management in the Mediterranean Sea. Fish and Fisheries 13, 60-88.
859 doi.org/10.1111/j.1467-2979.2011.00420.x.
860 Coll, M., Piroddi, C., Albouy, C., Ben Rais Lasram, F., Cheung, W.W.L., Christensen, V., Karpouzi,
861 V.S., Guilhaumon, F., Mouillot, D., Paleczny, M., Palomares, M.L., Steenbeek, J., Trujillo, P.,
862 Watson, R., Pauly, D., 2012. The Mediterranean Sea under siege: spatial overlap between
863 marine biodiversity, cumulative threats and marine reserves. Global Ecol. Biogeogr. 21, 465-
864 480. doi.org/10.1111/j.1466-8238.2011.00697.x.
865 Coll, M., Shannon, L.J., Kleisner, K.M., Juan-Jordá, M.J., Bundy, A., Akoglu, A.G., Bănaru, D.,
866 Boldt, J.L., Borges, M.F., Cook, A., Diallo, I., Fu, C., Fox, C., Gascuel, D., Gurney, L.GJ.,
867 Hattab, T., Heymans, J.J., Jouffre, D., Knight, B.R., Kucukavsar, S., Large, S.I., Lynam, C.,
868 Machias, A., Marshall, K.N., Masski, H., Ojaveer, H., Piroddi, C., Tam, J., Thiao, D., Thiaw,
869 M., Torres, M.A., Travers-Trolet, M., Tsagarakis, K., Tuck, I.,van der Meeren, G.I., Yemane,
870 D., Zador, S.G., Shin, Y.-J., 2016. Ecological indicators to capture the effects of fishing on
871 biodiversity and conservation status of marine ecosystems. Ecol. Indic. 60: 947-962.
872 doi:10.1016/j.ecolind.2015.08.048.
873 Collie, J.S., Botsford, L.W., Hastings, A., Kaplan, I.C., Largier, J.L., Livingston, P.A., Plaganyi, E.,
874 Rose, K.A., Wells, B.K., Werner, F.E., 2016. Ecosystem models for fisheries management:
875 finding the sweet spot. Fish and Fisheries 1-25. doi: 10.1111/faf.12093.

876 Cotté, C., d'Ovidio, F., Chaigneau, A., Lèvy, M., Taupier-Letage, I., Mate, B., Guinet, C., 2011.
877 Scale-dependent interactions of Mediterranean whales with marine dynamics. Limnol.
878 Oceanogr. 56(1), 219-232. doi:10.4319/lo.2011.56.1.0219.
879 CRPMEM PACA, 2016. Etat des lieux et caractérisation de la pêche maritime et des élevages
880 marins en PACA, 110 pp (In French).
881 Cury, P., Shannon, L., Shin, Y.J., 2003. The functioning of marine ecosystems: a fisheries
882 perspective. In: Sinclair, M., Valdimarsson, G. Eds. Responsible fisheries in the marine
883 ecosystem 103-124.
884 Dalsgaard, A.J.T., Pauly, D., Okey, T.A., 1997. Preliminary mass-balance model of Prince William
885 Sound, Alaska, for the pre-spill period, 1980-1989. Fish. Centre Res. Rep. 5(2), 1-34. doi:
886 10.14288/1.0074775.
887 Demaneche, S., Merrien, C., Berthou, P., Lespagnol, P., 2009. Rapport R3 Méditerranée
888 continentale, échantillonnage des marées au débarquement. Méthode d'élévation et évaluation
889 des captures et de l'effort de pêche des flottilles de la façade Méditerranée continentale sur la
890 période 2007-2008. Programme P6 AESYPECHE "Approche écosystémique de l'halieutique"
891 Projet Système d'Informations Halieutiques SIH, IFREMER, France, 54 pp (In French).
892 Diaz, F., Bănaru, D., Verley, P., Shin, Y., 2019. Implementation of an end-to-end model of the Gulf
893 of Lions ecosystem (NW Mediterranean Sea). II. Investigating the effects of high trophic
894 levels on nutrients and plankton dynamics and associated feedbacks. Ecol. Modell. 405, 51-
895 68. doi: 10.1016/j.ecolmodel.2019.05.004
896 Dickmann, M., 2005. Feeding ecology of sprat (*Sprattus sprattus* L.) and sardine (*Sardina*
897 *pilchardus* W.) larvae in the Baltic Sea and in the North Sea. PhD report Rostock University,
898 93 pp.
899 D'Ortenzio, F., Ribera d'Alcalà, M., 2009. On the trophic regimes of the Mediterranean Sea: a
900 satellite analysis. Biogeosciences 6, 139-148. https://doi.org/10.5194/bg-6-139-2009.

Dufau-Julliand, C., Marsaleix, P., Petrenko, A.A., Dekeyser I., 2004. Three-dimensional modelling of the Gulf of Lion's hydrodynamics (northwest Mediterranean) during January 1999 (MOOGLI3 Experiment) and late winter 1999: Western Mediterranean Intermediate Water's (WIW's) formation and its cascading over the shelf break. J. Geophys. Res. 109, C11002. doi: 10.1029/2003JC002019.

Farrugio, H., Alvarez Prado, F., Lleonart, J., De Ranieri, S., 1991. Etude pour l'aménagement et la gestion des pêches en Méditerranée occidentale. Rapport final Commission des Communautés Européennes, Contrat no. MA-1-232, 454 pp (In French).

Ferretti, F., Worm, B., Britten, G.L., Heithaus, M.R., Lotze, H.K., 2010. Patterns and ecosystem consequences of shark declines in the ocean. Ecol. Lett. 13, 1055–1071. doi:10.1111/j.1461-0248.2010.01489.x.

Fromentin, J.M., Farrugio, H., Deflorio, M., De Metrio, G., 2003. Preliminary results of aerial surveys of bluefin tuna in the Western Mediteraean sea. Col. Vol. Sci. Pap. ICCAT 55(3), 1019-1027.

Fu, C., Perry, I., Shin, Y.-J., Schweigert, J., Liu, H., 2013. An ecosystem modelling framework for incorporating climate regime shifts into fisheries management. Progr. Oceanogr. 115, 53–64. doi:10.1016/j.pocean.2013.03.003.

Fu, C., Olsen, N., Taylor, N., Grüss, A., Batten, S., Liu, H., Verley, P., Shin, Y.-J., 2017. Spatial and temporal dynamics of predator-prey species interactions off western Canada. ICES J. Mar. Sci. 74 (8), 2107-2119. doi.org/10.1093/icesjms/fsx056.

Fu, C., Travers-Trolet, M., Velez, L., Grüss, A., Bundy, A., Shannon, L.J., Fulton, E.A., Akoglu, E., Houle, J.E., Coll, M., Verley, P., Heymans, J.J., John, E., Shin, Y.-J. 2018. Risky business: the combined effects of fishing and changes in primary productivity on fish communities. Ecol. Modell. 368, 265-276. doi.org/10.1016/j.ecolmodel.2017.12.003.

925 Gernez, P., Antoine, D., Huot, Y., 2011. Diel cycles of the particulate beam attenuation coefficient
926 under varying trophic conditions in the northwestern Mediterranean Sea: Observations and
927 modeling. Limnol. Oceanogr. 56(1), 17-36. doi: 10.4319/lo.2011.56.1.0017.
928 GFCM-FAO, 2011a. Report of the SCSA working group on stock assessment of small pelagic
929 species, Campobello di Mazara, Italy, 1-6 November 2010.
930 GFCM-FAO, 2011b. Report of the working group on stock assessment of small pelagics species,
931 Chania, Greece, 24-29 october 2011.
932 Gifford, D.J., Caron, D.A., 1999. Sampling, preservation, enumeration and biomass of marine
933 protozooplankton. In: Harris, R.P., Wiebe, P.H., Lenz, J., Skjoldal, H.R., Huntley, M. (eds)
934 ICES Zooplankton Methodology Manual. Academic Press, London, 193-221.
935 Gregg, W.W., Casey, N.W., 2004. Global and regional evaluation of the SeaWiFS chlorophyll data
936 set. Remote Sens. Environ. 93, 463-479. doi:10.1016/j.rse.2003.12.012.
937 Grüss, A., Schirripa, M.J., Chagaris, D., Drexler, M., Simons, J., Verley, P., Shin, Y.-J., Karnauskas,
938 M., Oliveros-Ramos, R., Ainsworth, C.H., 2015. Evaluation of the trophic structure of the
939 West Florida Shelf in the 2000s using the ecosystem model OSMOSE. J. Mar. Syst. 144, 30–
940 47. doi: 10.1016/j.jmarsys.2014.11.004.
941 Grüss, A., Schirripa, M.J., Chagaris, D., Velez, L., Shin, Y.-J., Verley, P., Oliveros-Ramos, R.,
942 Ainsworth, C.H., 2016. Estimating natural mortality rates and simulating fishing scenarios for
943 Gulf of Mexico red grouper (*Epinephelus morio*) using the ecosystem model OSMOSE-WFS.
944 J. Mar. Syst. 154, 264–279. doi:10.1016/j.jmarsys.2015.10.014.
945 Halouani, G., Ben Rais Lasram, F., Shin Y.-J., Velez, L., Verley, P., Hattab, T., Oliveros-Ramos, R.,
946 Diaz, F., Ménard, F., Baklouti, M., Guyennon, A., Romdhane, M.S., Le Loc'h, F., 2016.
947 Modelling food web structure using an End-to-End approach in the coastal ecosystem of the
948 Gulf of Gabes (Tunisia). Ecol. Modell. 339, 45-57. doi:10.1016/j.ecolmodel.2016.08.008.
949 Härdsted-Roméo, M., 1982. Some aspects of the chemical composition of plankton from the NW
950 Mediterranean Sea. Mar. Biol. 70, 229-236.

951 Hastings, H.M., Conrad, M., 1979. Length and evolutionary stability of food chains. Nature 282,
952 838.
953 Helbing, D.,Brockmann, D., Chadefaux, T., Donnay, K., Blanke, U., Woolley-Meza, O., Moussaid,
954 M., Johansson, A., Krause, J., Schutte, S., Perc, M., 2015. Saving human lives: What
955 complexity science and information systems can contribute? J. Stat. Phys. 158, 735-781.
956 http://dx.doi.org/10.2139/ssrn.2390049.
957 Hermann M., Estournel C., Déqué M., Marsaleix P., Sevault F., Somot S., 2008. Dense water
958 formation in the Gulf of Lions shelf: Impact of atmospheric interannual variability and
959 climate change. Cont. Shelf Res. 28 (15), 2092-2112.
960 https://doi.org/10.1016/j.csr.2008.03.003.
961 Higginbottom, R., Hosie, G.W., 1989. Biomass and population structure of a large aggregation of
962 krill near Prydz Bay, Antarctica. Mar. Ecol. Prog. Ser. 58, 197-203.
963 Hu, Z.Y., Petrenko, A.A., Doglioli, A.M., Dekeyser, I., 2011a. Study of a mesoscale anticyclonic
964 eddy in the western part of the Gulf of Lion. J. Mar. Syst. 88, 3-11. doi:
965 10.1016/j.jmarsys.2011.02.008.
966 Hu, Z.Y., Petrenko, A.A., Doglioli, A.M., Dekeyser, I., 2011b. Numerical study of eddy generation
967 in the western part of the Gulf of Lions. J. Geophys. Res. C12, C12030.
968 doi:10.1029/2011JC007074.
969 Imbert, G., Bănaru, D., Delord, K., Dekeyser, I., Laubier, L., 2007. Apports de l'imagerie spatiale à
970 l'étude de la Thonaille dans les accalmies du mistral d'été. In « La Thonaille ou courantille
971 volante » final report to Regional Provence- Alpes- Cote d'Azur Council, France, IV:117-147
972 (In French).
973 Kaci, L., 2012. L'étude du régime alimentaire et de la forme des becs des céphalopodes dans le
974 golfe du Lion. Stage de Licence SNTE 3ème année, Aix-Marseille Université. 31 pp (In
975 French).
976 Kersalé, M., Petrenko, A.A., Doglioli, A.M., Dekeyser, I., Nencioli, F., 2013. Physical
977 characteristics and dynamics of the coastal Latex09 Eddy derived from in situ data and
978 numerical modeling. J. Geophys. Res. 118, 399-409. doi: 10.1029/2012JC008229.

979 Labat, J.-P., Cuzin-Roudy, J., 1996. Population dynamics of the krill *Meganyctiphanes norvegica*
980 (Sars) (Crustacea: Euphausiacea) in the Ligurian Sea (NW Mediterranean Sea). Size structure,
981 growth and mortality modelling. J. Plankton Res. 18: 2295-2312.
982 Labelle, M., Hoch, T., Liorzou, B., 1997. Analysis of the 1970-1995 bluefin sale records from
983 french seine catches in the Mediterranean. Col. Vol. Sci. Pap. ICCAT 46 (2): 140-149.
984 Laptikhovsky, V.V., Nigmatullin, C. M., 1993. Egg size, fecundity, and spawning in females of the
985 genus *Illex* (Cephalopoda: Ommastrephidae). ICES J. Mar. Sci. 50 (4), 393-403.
986 doi.org/10.1006/jmsc.1993.1044.
987 Le Bourg, B., Bănaru, D., Saraux, C., Nowaczyk, A., Le Luherne, E., Jadaud, A., Bigot, J. L.,
988 Richard, P., 2015. Trophic niche overlap of sprat and commercial small pelagic teleosts in the
989 Gulf of Lions (NW Mediterranean Sea). J. Sea Res. 103, 138-146.
990 http://dx.doi.org/10.1016/j.seares.2015.06.011.
991 Le Luherne, E., 2012. Etude de l'alimentation des maquereaux et des chinchards dans le Golfe du
992 Lion. Rapport de stage Master 2 professionnel Environnement Marin, Aix-Marseille
993 Université, 35 pp (In French).
994 Lévy, M., 2008. The modulation of biological production by oceanic mesoscale turbulence. Lecture
995 notes in Physics, Transport in Geophysical flow: Ten years after 744: 219-261.
996 Lleonart, J., 2001. Impact of fishery and environment on hake recruitment in Northwestern
997 Mediterranean – llucet. EU Contract FAIR n° CT-97-3522, Final Technical Report. 680 pp.
998 Lotze, H.K., Coll, M., Dunne, J., 2011. Historical changes in marine resources, foodweb structure
999 and ecosystem functioning in the Adriatic Sea. Ecosystems 14, 198-222.
1000 http://dx.doi.org/10.1007/s10021-010-9404-8.
1001 Ludwig, W., Dumont, E., Meybeck, M., Heussner, S., 2009. River discharges of water and nutrients
1002 to the Mediterranean and Black Sea: Major drivers for ecosystem changes during past and
1003 future decades? Progr. Oceanogr. 80 (3-4), 199–217.
1004 https://doi.org/10.1016/j.pocean.2009.02.001.

1005 Marsaleix, P., Auclair, F., Floor, J.W., Herrmann, M.J., Estournel, C., Pairaud, I., Ulses, C., 2008.
1006 Energy conservation issues in sigma-coordinate free-surface ocean models. Ocean Model. 20,
1007 61-89. doi: 10.1016/j.ocemod.2007.07.005.
1008 Marty, J.-C., Chiavérini, J., 2010. Hydrological changes in the Ligurian Sea (NW Mediterranean,
1009 DYFAMED site) during 1995–2007 and biogeochemical consequences. Biogeosciences 7,
1010 2117-2128. doi:10.5194/bg-7-2117-2010.
1011 Marty, J.-C., Chiavérini, J., Pizay, M.-D., Avril, B., 2002. Seasonal and inter-annual dynamics of
1012 nutrients and phytoplankton pigments in the western Mediterranean Sea at the DYFAMED
1013 time-series station (1991–1999). Deep Sea Res. II 49, 1965–1985. doi.org/10.1016/S0967-
1014 0645(02)00022-X.
1015 Marzloff, M., Shin, Y.-J., Tamb, J., Travers, M., Bertrand, A., 2009. Trophic structure of the
1016 Peruvian marine ecosystem in 2000–2006: Insights on the effects of management scenarios
1017 for the hake fishery using the IBM trophic model Osmose. J. Mar. Syst. 75, 290-304.
1018 doi:10.1016/j.jmarsys.2008.10.009.
1019 Mellon-Duval, C., de Pontual, H., Metral, L., Quemener, L., 2009. Growth of European hake
1020 (*Merluccius merluccius*) in the Gulf of Lions based on conventional tagging. ICES J. Mar.
1021 Sci. 67(1), 62-70. doi.org/10.1093/icesjms/fsp215.
1022 Mellon-Duval, C., Harmelin-Vivien, M., Métral, L., Loizeau, V., Mortreux, S., Roos, D., Fromentin,
1023 J.-M., 2017. Trophic ecology of the European hake in the Gulf of Lions, northwestern
1024 Mediterranean Sea. Sci. Mar. 81(1), 7-18. doi: 10.3989/scimar.04356.01A.
1025 Merquiol, L., 2016. Rapport de Master 1 sur l'alimentation et la condition du merlu européen,
1026 *Merluccius merluccius* (L., 1758), dans le Nord-Ouest de la Méditerranée : une comparaison
1027 2004-2015. 28 pp (In French).
1028 Millot, C., 1999. Circulation in the western Mediterranean Sea. J. Mar. Syst. 20 (1–4), 423–442.
1029 doi: 10.1016/S0924-7963(98)00078-5.

1030 Minas, M., Minas, H.J., 1989. Primary production in the gulf of Lions with considerations to the
1031 Rhone River input. Water Pollution Research Reports 13, 112-125.
1032 Niewiadomska, K., Claustre, H., Prieur, L., d'Ortenzio, F., 2008. Submesoscale physical-
1033 biogeochemical coupling across the Ligurian current (northwestern Mediterranean) using a
1034 bio-optical glider. Limnol. Oceanogr. 53(2), 2210–2225. doi: 10.2307/40058379.
1035 Odum, E.P., 1959. Fundamentals of ecology. Second edition. In collaboration with H.T. Odum.
1036 Philadelphia, Saunders, XVII, 546 pp.
1037 Oliveros-Ramos, R., Shin, Y.-J., 2016. Calibrar: an R package for fitting complex ecological
1038 models. ArXiv Prepr. ArXiv160303141.
1039 Oliveros-Ramos, R., Verley, P., Shin, Y.-J., 2015. A sequential approach to calibrate ecosystem
1040 models with multiple time series data. ArXiv Prepr. ArXiv150906123.
1041 Ouillon, S., Petrenko, A., 2005. Above-water measurements of reflectance and chlorophyll-a
1042 algorithms in the Gulf of Lions, NW Mediterranean Sea. Opt. Express 13, 2531-2548.
1043 doi.org/10.1364/OPEX.13.002531.
1044 Palomares, M.L.D., Pauly, D., 1998. Predicting food consumption of fish populations as functions
1045 of mortality, food type, morphometrics, temperature and salinity. Mar. Freshw. Res. 49 (5),
1046 447–453. doi.org/10.1071/MF98015.
1047 Pauly, D., Christensen, V., Dalsgaard, A., Froese, R., Torres, J., 1998. Fishing down marine food
1048 webs. Science 279 (5352), 860–863. doi: 10.1126/science.279.5352.860.
1049 Pethybridge, H., Bodin, N., Arsenault-Pernet, E.J., Bourdeix, J.H., Brisset, B., Bigot, J.L., Roos, D.,
1050 Peter, M., 2014. Temporal and inter-specific variations in forage fish feeding conditions in the
1051 NW Mediterranean: lipid content and fatty acid compositional changes. Mar. Ecol. Prog. Ser.
1052 512, 39-54. doi.org/10.3354/meps10864.
1053 Petrenko, A., 2003. Variability of circulation features in the Gulf of Lions NW Mediterranean Sea.
1054 Importance of inertial currents. Oceanol. Acta 26, 323-338. doi: 10.1016/S0399-
1055 1784(03)00038-0.

1056 Piroddi, C., Coll, M., Liquete, C., Macias, D., Greer, K., Buszowski, J., Steenbeek, J., Danovaro, R.,
1057 Christensen, V., 2017. Historical changes of the Mediterranean Sea ecosystem: modelling the
1058 role and impact of primary productivity and fisheries changes over time. Sci. Rep. 7, 44491.
1059 doi:10.1038/srep44491.
1060 Qúero, J.-C., Vayne, J.-J., 1997. Les poissons de mer des pêches françaises. Eds. Delachaux Et
1061 Niestĺe, 304 pp.
1062 Reed, J., Shannon, L.J., Velez, L., Akoglu, E., Bundy, A., Coll, M., Fu, C., Fulton, E.A., Grüss, A.,
1063 Halouani, G., Heymans, J.J., Houle, J., John, E., Le Loc'h, F., Salihoglu, B., Verley, P., Shin,
1064 Y.-J. 2017. Ecosystem indicators – accounting for variability in species' trophic levels. ICES
1065 J. Mar. Sci. 74(1), 158-169. doi.org/10.1093/icesjms/fsw150.
1066 Rose, K., Allen, J.U., Artioli, Y. , Barange, M., Blackford, J., Carlotti, F., Cropp, R., Daewel, U.,
1067 Edwards, K., Flynn, K., Hill, SL., HilleRisLambers, R., Huse, G., Mackinson, S., Megrey, B.,
1068 Moll, A., Rivkin, R., Salihoglu, B., Schrum, C., Shannon, L., Shin, Y.-J., Smith, S.L.,
1069 Solidoro, C., St. John, M., Zhou, M., 2010. End-To-End Models for the Analysis of Marine
1070 Ecosystems: Challenges, Issues, and Next Steps. Mar. Coast. Fish.2, 115-130.
1071 doi.org/10.1577/C09-059.1.
1072 Rose, K., 2012. End-to-end models for marine ecosystems: Are we on the precipice of a significant
1073 advance or just putting lipstick on a pig? Sci. Mar. 76(1), 195-201. doi:
1074 10.3989/scimar.03574.20B.
1075 Ross, R.M., Quetin, L.B., 1986. How Productive are Antarctic Krill? Bioscience 36, 264–269.
1076 Rossi, S., Sabate, A., Latasa, S.M., Reyes, E., 2006. Lipid biomarkers and trophic linkages between
1077 phytoplankton, zooplankton and anchovy (*Engraulis encrasicolus*) larvae in the NW
1078 Mediterranean. J.Plankton Res. 28(6), 551-562. doi.org/10.1093/plankt/fbi140.
1079 Royer, F., Fromentin, J.M., Gaspar, P., 2004. Association between bluefin tuna schools and oceanic
1080 features in the western Mediterranean. Mar. Ecol. Prog. Ser. 269, 249-263. doi :
1081 10.3354/meps269249.

1082 Sacchi, J., 2008. Impact des techniques de pêche sur l'environnement en Méditerranée. GFCM
1083 Stud. Rev. 84, 1-82.
1084 Sánchez, P., González, A.F., Jereb, P., Laptikhovsky, V.V., Mangold, K.M., Nigmatullin, Ch.M.,
1085 Ragonese, S., 1998. *Illex coindetii*, p 18. In: FAO Fish. Tech. Pap. 376 pp.
1086 Santojanni, A., Cingolani, N., Arneri, E., Kirikwood, G., Belardinelli, A., Giannetti, G., Colella, S.,
1087 Donato, F., Barry, C., 2005. Stock assessment of sardine (*Sardina pilchardus*, Walb.) in the
1088 Adriatic Sea, with an estimate of discards. Sci. Mar. 69, 603-617.
1089 doi.org/10.3989/scimar.2005.69n4603.
1090 Sara, G., Sara, R., 2007. Feeding habits and trophic levels of bluefin tuna *Thunnus thynnus* of
1091 different size classes in the Mediterranean Sea. J. Appl. Ichthyol. 23, 122–127.
1092 doi.org/10.1111/j.1439-0426.2006.00829.x.
1093 SCRS, 1997. Report of the ICCAT SCRS Bluefin tuna stock assessment session. Collect. Vol. Sci.
1094 Pap. ICCAT 46(1), 1-186.
1095 Shin, Y.-J., Cury, P., 2001. Exploring fish community dynamics through size-dependent trophic
1096 interactions using a spatialized individual-based model. Aquat. Living Resour. 14(2), 65-80.
1097 doi.org/10.1016/S0990-7440(01)01106-8.
1098 Shin, Y.-J., Cury, P., 2004. Using an individual-based model of fish assemblages to study the
1099 response of size spectra to changes in fishing. Can. J. Fish. Aquat. Sci. 61, 414-431.
1100 doi.org/10.1139/f03-154.
1101 Shin, Y.-J., Shannon, L.J., Cury, P.M., 2004. Simulations of fishing effects on the southern Benguela
1102 fish community using an individual-based model: learning from a comparison with ECOSIM.
1103 In Ecosystem Approaches to Fisheries in the Southern Benguela. Shannon, L.J., Cochrane,
1104 K.L. and S.C. Pillar (Eds.). Afr. J. Mar. Sci. 26, 95-114.
1105 doi.org/10.2989/18142320409504052.

1106 Shin, Y.-J., Travers, M., Maury, O., 2010. Coupling models of low and high trophic levels models:
1107 towards a pathways-orientated approach for end-to-end models. Progr. Oceanogr. 84, 105-
1108 112. doi.org/10.1016/j.pocean.2009.09.012.
1109 Shin, Y.-J., Houle, J.E., Akoglu, E., Blanchard, J., Bundy, A., Coll, M., Demarcq, H., Fu, C., Fulton,
1110 E.A., Heymans, J.J., Salihoglu, B., Shannon, L.J., Sporcic, M., Velez, L., 2018. The
1111 specificity of marine ecological indicators to fishing in the face of environmental change: a
1112 multi-model evaluation. Ecol. Indic. 89, 317-326.
1113 https://doi.org/10.1016/j.ecolind.2018.01.010.
1114 Sieburth, J.McN., Jiirgen Lenx V.S., 1978. Pelagic ecosystem structure: Heterotrophic
1115 compartments of the plankton and their relationship to plankton size fractions. Limol.
1116 Oceanogr. 23(6), 1256-1263.
1117 Siegel, D.A., Doneys S.C, Yoder J.A., 2002. The North Atlantic Spring Phytoplankton Bloom and
1118 Sverdrup's Critical Depth Hypothesis. Science, 296, 730-733. doi:10.1126/science.1069174.
1119 Sinovčić, G., Franičević, M., Zorica, B., Čikeš-Keč, V., 2004. Length-weight and length-length
1120 relationships for 10 pelagic fish species from the Adriatic Sea (Croatia). J. Appl. Ichthyol.
1121 20(2), 156-158. doi.org/10.1046/j.1439-0426.2003.00519.x.
1122 Smith, ADM., Brown, C.J., Bulman, C.M., Fulton, E.A., Johnson, P., Kaplan, I.C., Lozano-Montes,
1123 H., Mackinson, S., Marzloff, M., Shannon, LJ., Shin, Y.-J., Tam, J., 2011. Impacts of fishing
1124 low–trophic level species on marine ecosystems. Science 333, 1147–1150. doi:
1125 10.1126/science.1209395.
1126 Stergiou, K.I., Karpouzi, V.S., 2002. Feeding habits and trophic levels of Mediterranean fish. Rev.
1127 Fish Biol. Fish. 11 (3), 217–254.
1128 Travers, M., Shin, Y.-J., Jennings, S., Cury, P., 2007. Towards end-to-end models for investigating
1129 the effects of climate and fishing in marine ecosystems. Progr. Oceanogr. 75 (4), 751-770.
1130 doi.org/10.1016/j.pocean.2007.08.001.

1131 Travers, M., Shin, Y.-J., Jennings, S., Machu, E., Huggett, J.A., Field, J.G., Cury, P.M., 2009. Two-
1132 way coupling versus one-way forcing of plankton and fish models to predict ecosystem
1133 changes in the Benguela. Ecol. Modell. 220, 3089–3099.
1134 doi:10.1016/j.ecolmodel.2009.08.016.
1135 Travers, M., Shin, Y.-J., Shannon, L.J., Cury, P., 2006. Simulating and testing the sensitivity of
1136 ecosystem-based indicators to fishing in the southern Benguela ecosystem. Can. J. Fish.
1137 Aquat. Sci. 63, 943-956. doi.org/10.1139/F06-003.
1138 Travers, M., Watermeyer, K., Shannon, L.J., Shin, Y.-J., 2010. Changes in food web structure under
1139 scenarios of overfishing in the Southern Benguela: Comparison of the Ecosim and OSMOSE
1140 modelling approaches. J. Mar. Syst. 79, 101-111. doi: 10.1016/j.jmarsys.2009.07.005.
1141 Travers–Trolet, M., Shin, Y.-J., Shannon, L.J., Moloney, C.L., Field, J.G., 2014. Combined Fishing
1142 and Climate Forcing in the Southern Benguela Upwelling Ecosystem: An End-to-End
1143 Modelling Approach Reveals Dampened Effects. PLoS ONE 9, e94286.
1144 doi:10.1371/journal.pone.0094286.
1145 Ulses, C., Estournel, C., Durrieu de Madron, X., Palanques A., 2008. Suspended sediment transport
1146 in the Gulf of Lions (NW Mediterranean): Impact of extreme storms and floods. Cont. Shelf
1147 Res. 28, 2048-2070. http://dx.doi.org/10.1016/j.csr.2008.01.015.
1148 Van Beveren, E., Bonhommeau, S., Fromentin, J.M., Bigot, J.L., Bourdeix, J.H., Brosset, P., Roos,
1149 D., Saraux, C., 2014. Rapid changes in growth, condition, size and age of small pelagic fish in
1150 the Mediterranean. Mar. Biol. 161, 1809-1822. doi : 10.1007/s00227-014-2463-1.
1151 Volpe, G., Santoleri, R., Vellucci, V., Ribera d'Alcala, M., Marullo, S., D'Ortenzio, F., 2007. The
1152 colour of the Mediterranean Sea: Global versus regional bio-optical algorithms evaluation and
1153 implication for satellite chlorophyll estimates. Remote Sens. Environ. 107, 625-638. doi:
1154 10.1016/j.rse.2006.10.017.

1155 Yemane, D., Shin, Y.-J., Field, J.G., 2009. Exploring the effect of Marine Protected Areas on the
1156 dynamics of fish communities in the southern Benguela: an individual-based modelling
1157 approach. ICES J. Mar. Sci. J. Cons. 66, 378–387. doi:10.1093/icesjms/fsn171.
1158 Walsh, J.J., 1981. A carbon budget for overfishing off Peru. Nature 290(5804), 300.
1159 http://sih.ifremer.fr/(December 2017)
1160 www.fishbase.org
1161 www.osmose-model.org
1162
1163

LEGENDS OF TABLES

Table 1 Characteristics and parameters of the five LTL groups of the Eco3M-S model.

Table 2 Parameter values of the OSMOSE-GoL model obtained from fitting the model to observed data. M_0: larval mortality rate; M_s: mortality rate due to predation from other species that are not explicitly considered in the model; F: annual fishing mortality rate; a_p: availability coefficients of plankton groups to HTL species.

Table 3 Size classes of the different species implemented in the OSMOSE-GoL model, minimum and maximum predator/prey size ratios. MIR= Maximum ingestion rate.

Table 4 Input parameters of the OSMOSE-GoL model for each of the 10 HTL species modelled. K (growth rate), L_∞ (asymptotic size) and t_0 (time at null size): the von Bertalanffy growth parameters; b: the exponent of the allometric length–weight relationship; c: constant of proportionality of the allometric length-weight relationship; s_{mat}: size at maturity; φ: relative fecundity; S: egg size; a_{max}: longevity; s_{rec}: legal size of recruitment for fisheries catch.

Table 5 Seasonality of the fishing activity in the GoL for target species.

Table 1

	Size range (µm)	Eco3M-S mortality rate, m_p (d^{-1})	Trophic level	Conversion factor (mg_{ww} $mmolN^{-1}$)
NANOPHY	2-20[a]	0.000[b]	1.0[c]	993.75[d,e,f]
MICROPHY	20-200[a]	0.075[b]	1.0[c]	993.75[d,e,f]
NANOZOO	5-20[a]	0.043[b]	1.5[c]	832.50[g,h]
MICROZOO	2-200[a]	0.070[b]	2.0[c]	832.50[g,h]
MESOZOO	200-2000[a]	0.033*[,b]	2.5[c]	150.00**[,g]

*Units: m^3 $mmolC^{-1}$ d^{-1} (predation rate), **Units: mg_{ww} $mmolC^{-1}$, [a]Sieburth et al. (1978), [b]Campbell et al. (2013), [c]Arbitrarily set, [d]Dalsgaard and Pauly (1997), [e]Walsh (1981), [f]Bundy (2004), [g]Gifford and Caron (2000), [h]Hardsted-Roméo (1982).

1191 **Table 2**

Species	Mortality			Availability coefficients
	M_0 (y^{-1})	M_s (y^{-1})	F (y^{-1})	a_p
Northern krill	7.555	0.237	0.000	-
Southern shortfin squid	5.238	0.698	1.253	-
European pilchard	5.558	0.365	0.082	-
European anchovy	6.609	0.228	0.185	-
European sprat	4.549	0.404	0.000	-
Atlantic horse mackerel	1.271	0.061	0.419	-
Atlantic mackerel	9.878	0.991	0.548	-
Blue whiting	6.731	0.604	0.013	-
European hake	10.959	0.285	0.122	-
Atlantic bluefin tuna	0.000	0.000	0.642	-
NANOPHY	-	-	-	0.591
MICROPHY	-	-	-	0.223
NANOZOO	-	-	-	0.311
MICROZOO	-	-	-	0.157
MESOZOO	-	-	-	0.148

1192

1193

1194 **Table 3**

Species	Size classes (cm)	Predator/prey size ratios		MIR
		Min	Max	
Northern krill	-	188	4	5.0
Southern shortfin squid	-	17	1	5.92
European pilchard	<3	65	13	8.0
	3-12.5	1139	15	
	>12.5	1621	60	
European anchovy	<3	500	4	4.49
	3-8	500	4	
	>8	806	7	
European sprat	<3	500	2	4.58
	3-11.6	517	10	
	>11.6	517	10	
Atlantic horse mackerel	<16	40	4	2.54
	>16	100	4	
Atlantic mackerel	<20	100	1	5.0
	>20	61	2	
Blue whiting	<15	40	3	5.92
	>15	32	4	
European hake	<36	9	1	6.76
	>36	14	1	
Atlantic bluefin tuna	-	20	4	7.95

1195

Table 4

Species	Growth					Reproduction				
	K (y^{-1})	L_∞ (cm)	t_0 (y)	b	c (g cm^{-3})	s_{mat} (cm)	φ (egg g^{-1})	S (cm)	a_{max} (y)	s_{rec} (cm)
Northern krill	1.680	3.462	-0.2	3.16	7.38E-03	1.05	7547	0.06	1	0
Southern shortfin squid	0.930	17.400	0.087	2.12	8.96E-02	11.50	420	0.08	3	10
European pilchard	0.334	19.925	-2.164	3.25	3.8E-03	12.50	2157	0.1	7	10
European anchovy	0.609	16.29	-1.396	3.02	6.5E-03	11.00	1271	0.1	4	11
European sprat	0.370	14.20	-2.3	2.51	2.26E-02	11.40	1096	0.12	6	10
Atlantic horse mackerel	0.230	39.90	-0.94	2.84	1.3E-02	16.00	286	0.08	9	15
Atlantic mackerel	0.370	42.00	-0.50	3.13	6.7E-03	30.00	300	0.12	12	18
Blue whiting	0.230	40.50	-1.27	3.00	6.4E-03	15.00	1217	0.12	7	16
European hake	0.150	68.00	-0.47	3.03	1.0E-02	36.00	320	0.12	20	20
Atlantic bluefin tuna	0.093	318.85	-0.97	3.0092	1.96E-05	97.50	0	-	20	80

Table 5

Fishing mortality / time steps	Southern shortfin squid	European pilchard	European anchovy	Atlantic horse mackerel	Atlantic mackerel	Blue whiting	European hake	Atlantic bluefin tuna
1, 2	0.042	0.024	0.048	0.026	0.042	0.017	0.014	0.000
3, 4	0.042	0.028	0.040	0.027	0.042	0.048	0.040	0.005
5, 6	0.042	0.038	0.042	0.046	0.042	0.125	0.059	0.041
7, 8	0.042	0.035	0.042	0.066	0.042	0.119	0.049	0.070
9, 10	0.042	0.044	0.050	0.062	0.042	0.113	0.057	0.052
11, 12	0.042	0.063	0.049	0.053	0.042	0.053	0.056	0.054
13, 14	0.042	0.068	0.038	0.029	0.042	0.008	0.053	0.050
15, 16	0.042	0.063	0.039	0.031	0.042	0.003	0.058	0.120
17, 18	0.042	0.052	0.046	0.048	0.042	0.004	0.055	0.096
19, 20	0.042	0.040	0.042	0.052	0.042	0.003	0.039	0.013
21, 22	0.042	0.028	0.040	0.040	0.042	0.004	0.020	0.000
23, 24	0.042	0.017	0.026	0.022	0.042	0.003	0.005	0.000

1202 LEGENDS OF FIGURES

1203

1204 **Fig. 1.** Processes taken into account within each of the two models and processes linking the two
1205 models (dashed-line arrows). The time step of Eco3M-S/SYMPHONIE (left hand side, Campbell *et*
1206 *al.*, 2013) is one hour while that of OSMOSE (right hand side, adapted from Travers-Trolet *et al.*,
1207 2014) is 15 days. The two-ways coupling mode is used throughout the predation process, where the
1208 biomass of the plankton groups serve as prey field for fish schools, cephalopods and krill ("Prey
1209 availability" arrow), while an explicit rate of HTL-induced predation is specifically applied as
1210 feedback on each of the aforementioned five plankton groups ("Predation mortality" arrow). In the
1211 one-way forcing mode, plankton biomasses serve as prey fields to fish schools, cephalopods and
1212 krill ("Prey availability" arrow), without any feedback on the plankton prey compartments.

1213

1214 **Fig. 2.** The Eco3M-S/Symphonie model domain in the NW Mediterranean Sea is delineated by the
1215 black thin line. The OSMOSE-GoL model domain over the Gulf of Lions is delimited by the black
1216 bold line. The map of grid points in the OSMOSE-GoL domain is given in the small panel in the
1217 right edge of the figure. The black arrow indicates the main flow of the Northern Current (NC).
1218 Rivers taken into account by the model are named. Bathymetry with isobaths 50, 100 and 1000 m is
1219 shown in the modeled area.

1220

1221 **Fig. 3.** Temporal patterns of change in the simulated biomass of the 10 HTL species during the last
1222 four years of spin-up over the whole modeled domain. The solid blue line shows the median value
1223 computed from the 50 simulation replicates. The lower and upper limits of the grey range delineate
1224 the 0.25 and 0.75 (resp.) percentiles computed from the 50 replicates. The two horizontal dotted
1225 black lines represent the range of observed biomass (see references 2.3).

1226

1227 **Fig. 4.** Temporal patterns of change in the simulated landings of the 10 HTL species during the last

four years of spin-up over the whole modeled domain. The solid blue line shows the median value computed from the 50 simulation replicates. The lower and upper limits of the grey range delineate the 0.25 and 0.75 percentiles computed from the 50 simulation replicates. The horizontal black lines represent monthly observed landings (see references 2.3).

Fig. 5. Time-series of satellite-derived (blue) and modeled (red) chlorophyll surface concentrations (mg m^{-3}) over the whole modeled domain. Thick lines represent mean values and shaded area (grey) is the range of error bars computed from the GlobColour algorithm. Missing data in the time-series are explained by cloudy days without any useable pixels.

Fig. 6. Time-series of the averaged error (mg m^{-3}) on satellite-derived chlorophyll (blue dots) and of the C parameter (metric of data-to-model distance in mg m^{-3}, red dots) on the whole modeled domain.

Fig. 7. Mean diet (over the years 36 to 43) of larvae, juveniles and adults of the 10 HTL species considered in the OSMOSE-GoL model.

Fig. 8. Representation of the trophic levels and the main fluxes of matter between the compartments of the OSMOSE-GoL model (TL = trophic level, LTL = low trophic levels, HTL = high trophic levels). Size of the arrows is related to the intensity of predation fluxes. Fluxes lower than 10 tons y^{-1} are not quoted in the diagram. For sake of clarity, only fluxes that account for at least 10% of predation total flux for a given prey are shown.

Fig. 9. Trophic levels *vs*. total length of the ten HTL species represented in the OSMOSE-GoL model (there was a high inter-annual overlap of the trophic levels). Horizontal dashed black lines indicate the minimum and maximum values from the literature data based on the analysis of

1254 stomach content and corresponding to a range of total length. Horizontal solid black lines indicate
1255 the trophic levels from the ECOPATH model of the GoL (Bănaru *et al*., 2013).
1256

1257 **Fig**

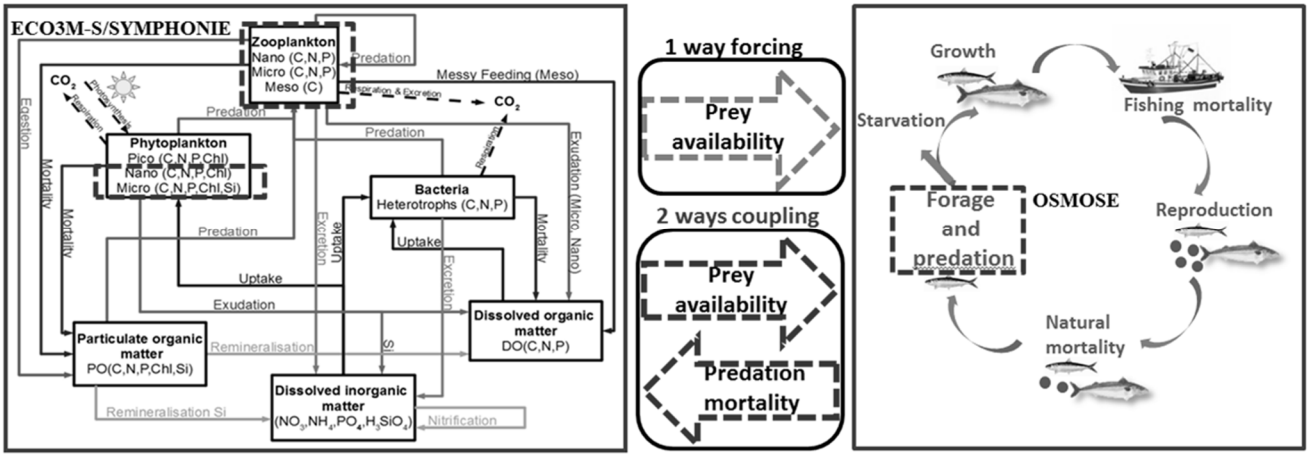

1258

1259

Fig. 2.

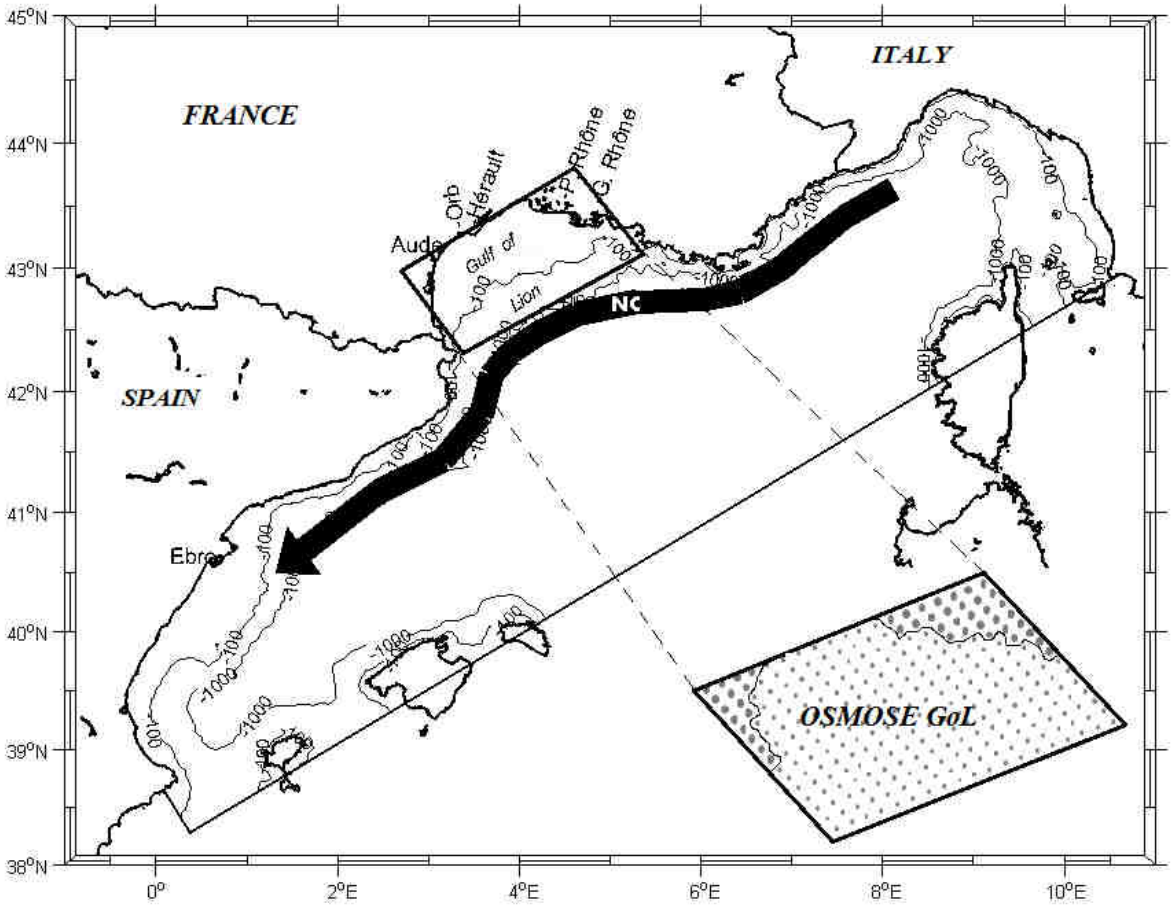
FRANCE
ITALY
SPAIN
Aude
Orb
Hérault
P. Rhône
G. Rhône
Gulf of Lion
Nc
Ebre
OSMOSE GoL
45°N
44°N
43°N
42°N
41°N
40°N
39°N
38°N
0°
2°E
4°E
6°E
8°E
10°E

1263 **Fig. 3.**

1264

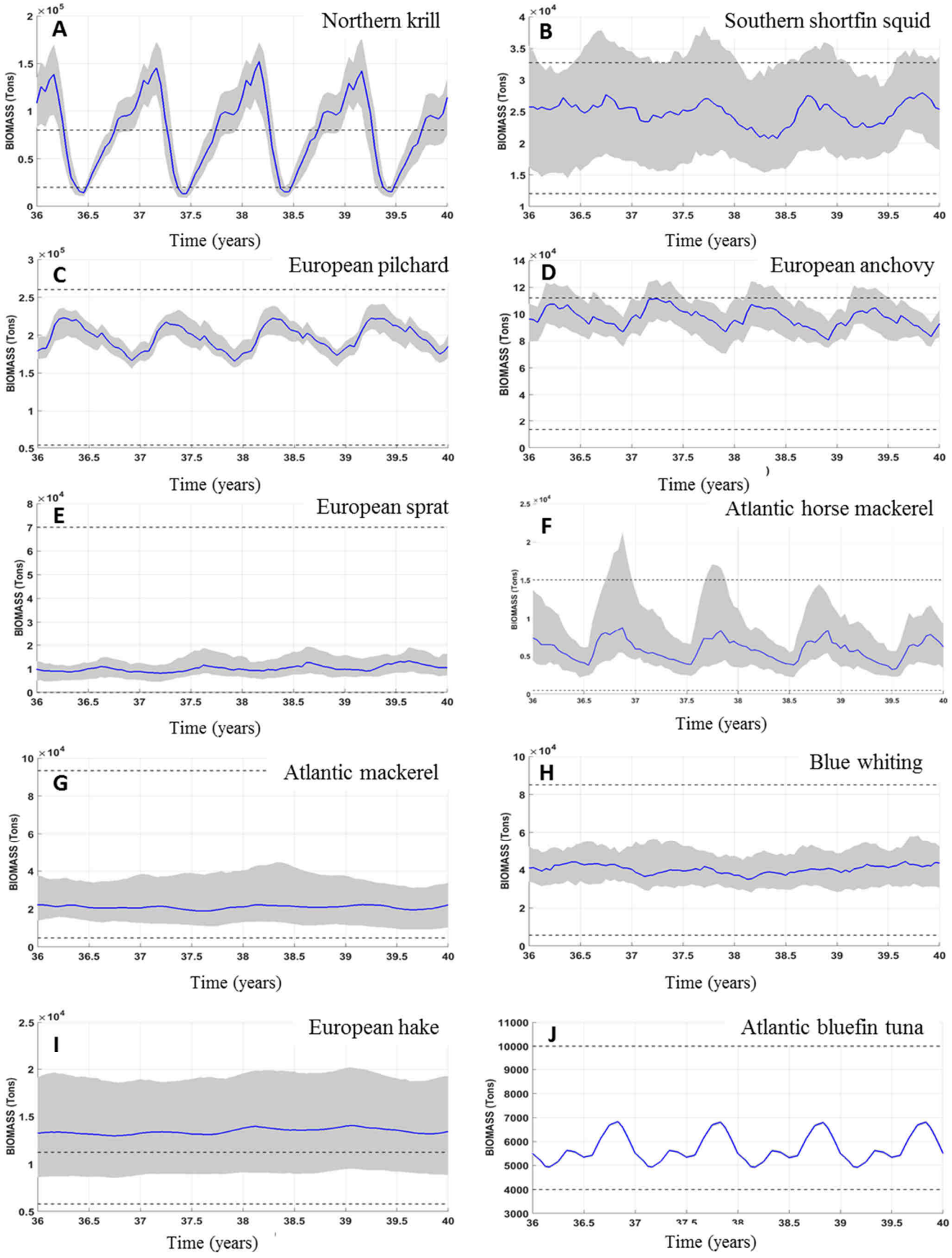

1265

1266 **Fig. 4.**

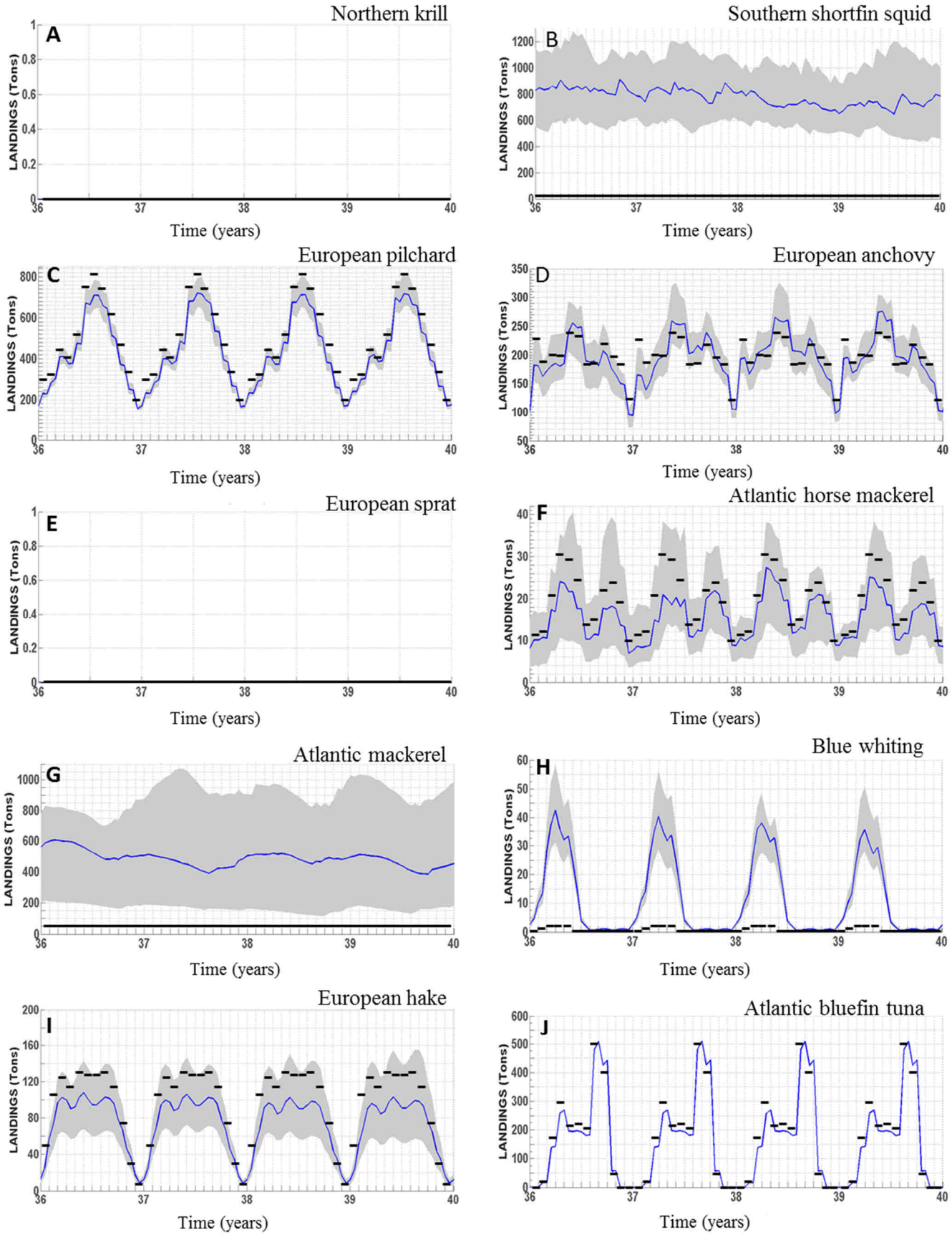

1267

1268

Fig. 5.

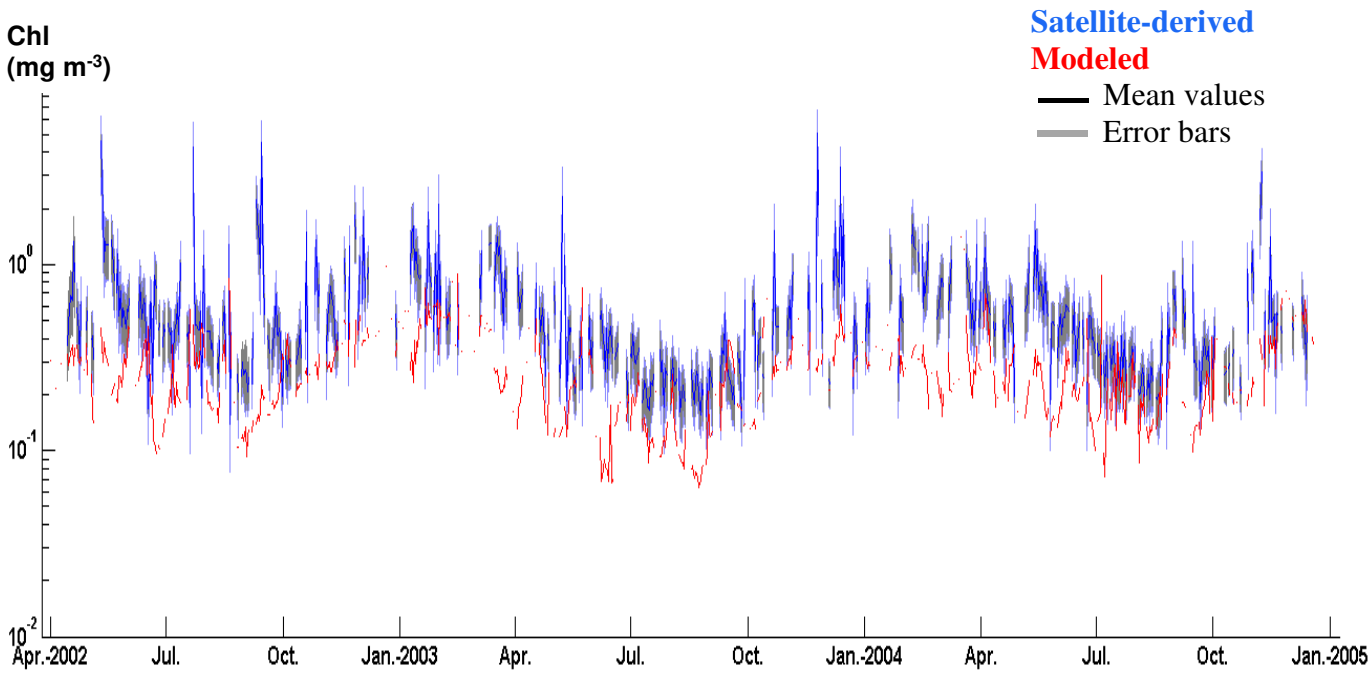
Chl
(mg m-3)
Satellite-derived
Modeled
Mean values
Error bars
10^0
10^-1
10^-2
Apr.-2002
Jul.
Oct.
Jan.-2003
Apr.
Jul.
Oct.
Jan.-2004
Apr.
Jul.
Oct.
Jan.-2005

Fig. 6.

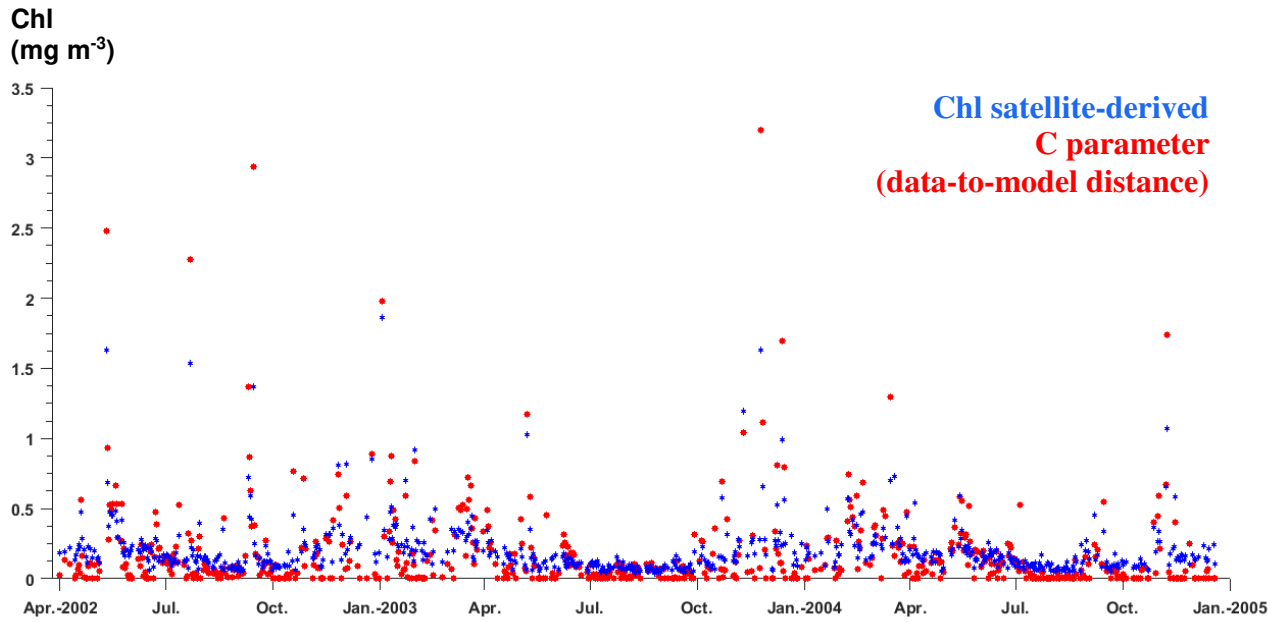
Chl
(mg m-3)
3.5
3
2.5
2
1.5
1
0.5
0
Apr.-2002
Jul.
Oct.
Jan.-2003
Apr.
Jul.
Oct.
Jan.-2004
Apr.
Jul.
Oct.
Jan.-2005
Chl satellite-derived
C parameter
(data-to-model distance)

1283 **Fig. 7.**

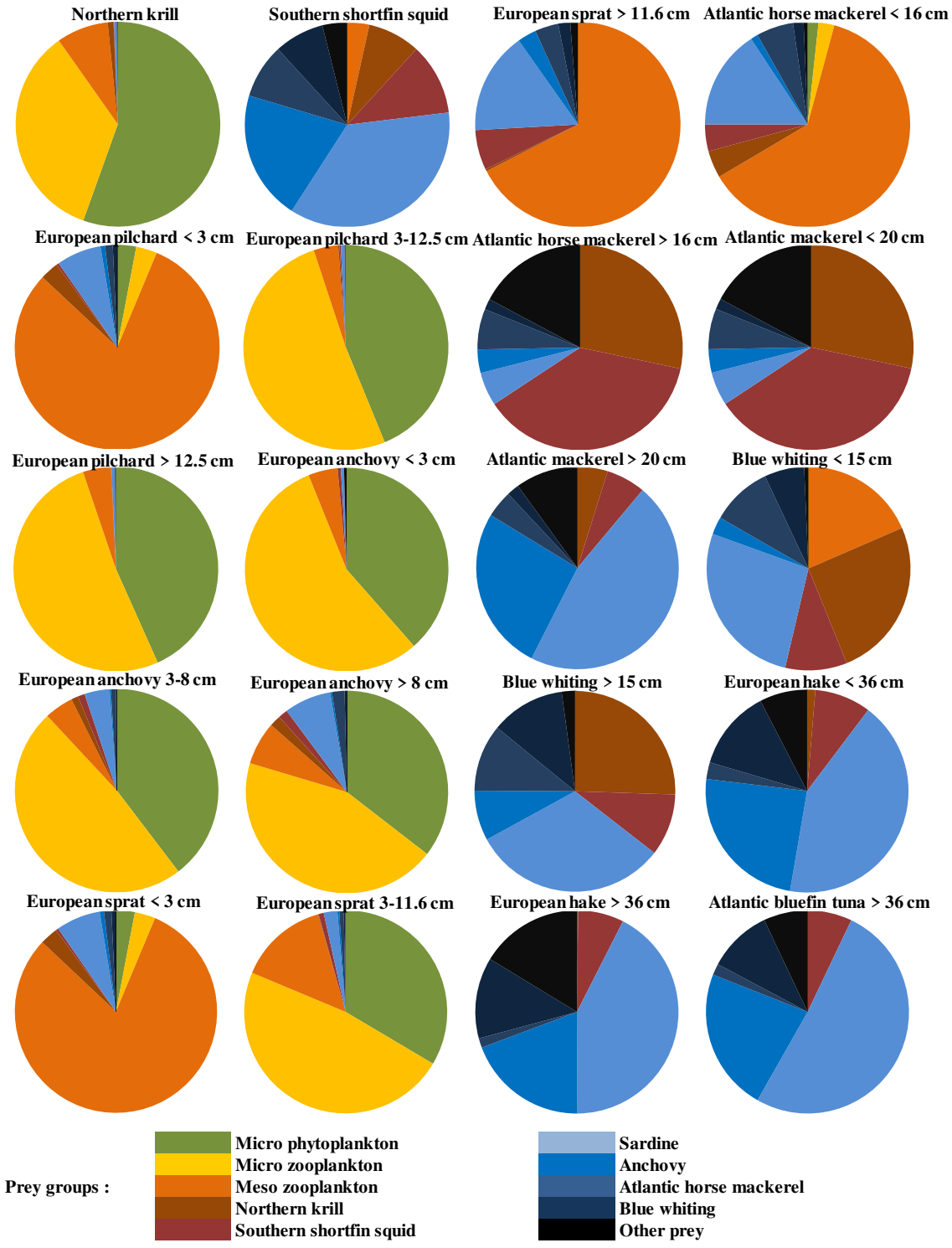

1284

1285

1286

Fig. 8.

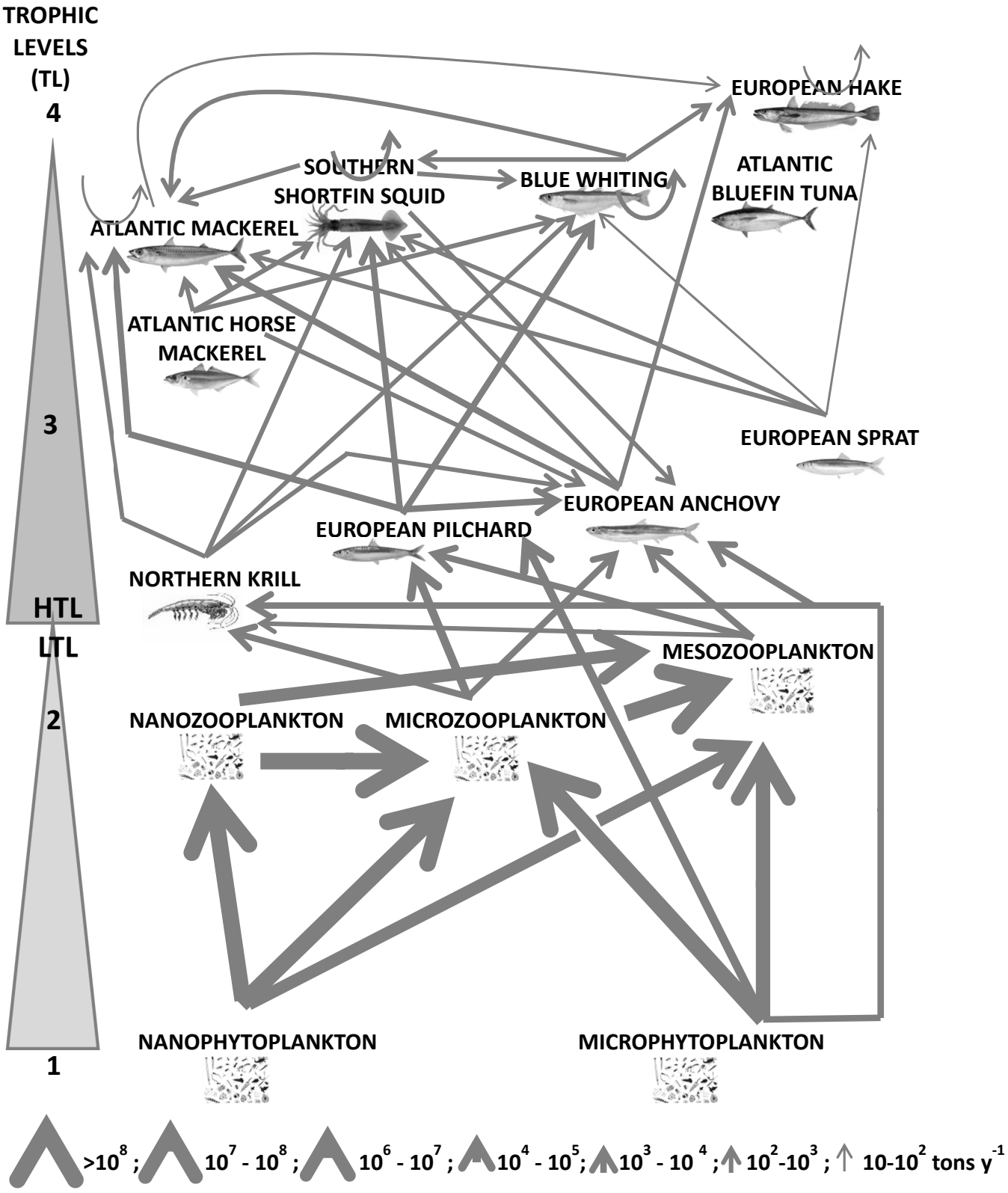
TROPHIC LEVELS (TL)
4
3
HTL
LTL
2
1
EUROPEAN HAKE
SOUTHERN SHORTFIN SQUID
BLUE WHITING
ATLANTIC BLUEFIN TUNA
ATLANTIC MACKEREL
ATLANTIC HORSE MACKEREL
EUROPEAN SPRAT
EUROPEAN ANCHOVY
EUROPEAN PILCHARD
NORTHERN KRILL
MESOZOOPLANKTON
NANOZOOPLANKTON
MICROZOOPLANKTON
NANOPHYTOPLANKTON
MICROPHYTOPLANKTON
>10^8 ; 10^7 - 10^8 ; 10^6 - 10^7 ; 10^4 - 10^5; 10^3 - 10^4 ; 10^2-10^3 ; 10-10^2 tons y^-1

1314 **Fig. 9.**

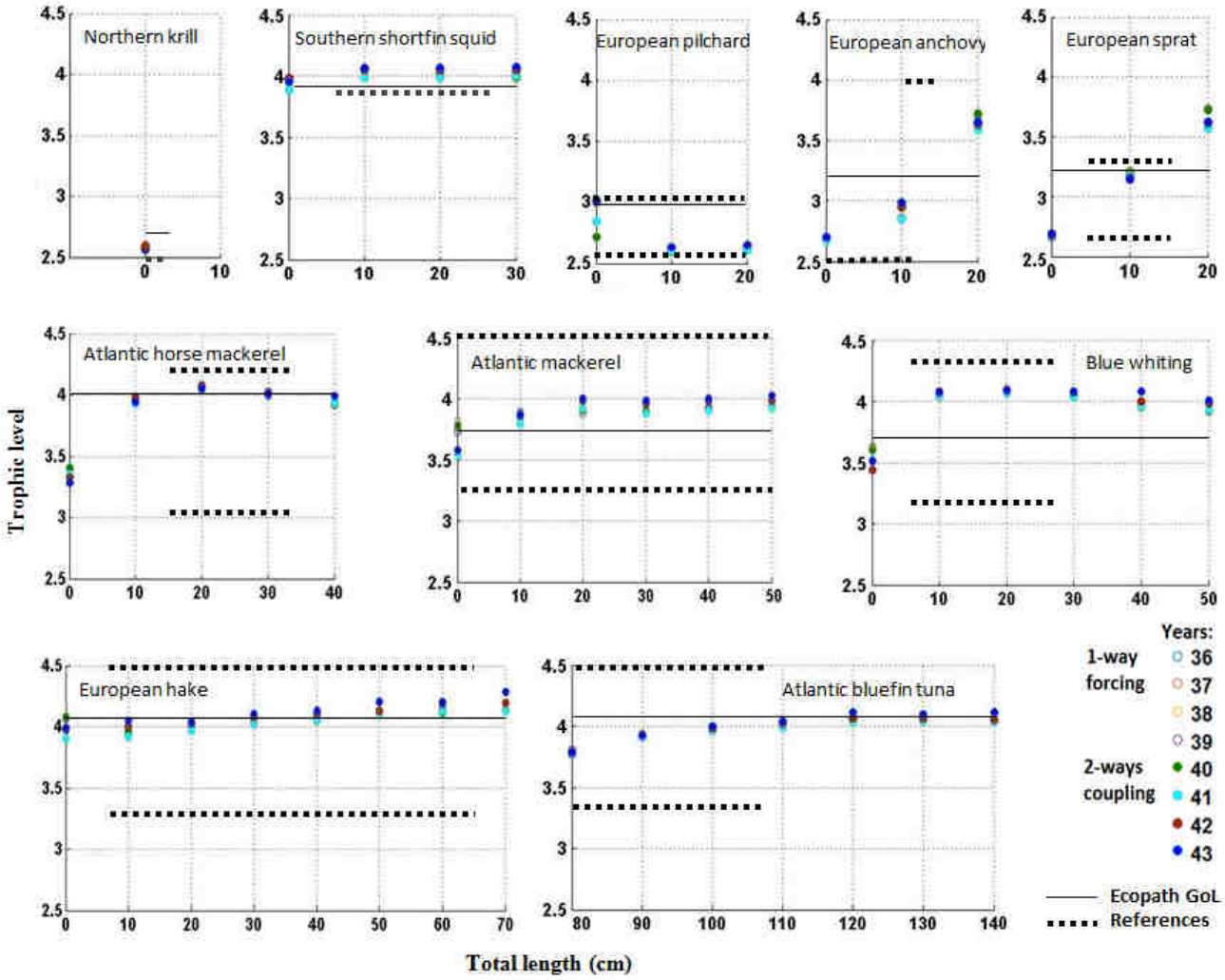

1315